



# Dust reddening in star-forming galaxies

Ting Xiao,<sup>★</sup> Tinggui Wang,<sup>★</sup> Huiyuan Wang, Hongyan Zhou, Honglin Lu and Xiaobo Dong

Key Laboratory for Research in Galaxies and Cosmology, Department of Astronomy, University of Science & Technology of China, Chinese Academy of Sciences, Hefei, Anhui 230026, China

Accepted 2011 December 2. Received 2011 November 30; in original form 2011 June 2

## ABSTRACT

We present empirical relations between the global dust reddening and other physical galaxy properties including the H $\alpha$  luminosity, H $\alpha$  surface brightness, metallicity and axial ratio for star-forming disc galaxies. The study is based on a large sample of  $\sim 22\,000$  well-defined star-forming galaxies selected from the Sloan Digital Sky Survey. The reddening parametrized by colour excess  $E(B - V)$  is derived from the Balmer decrement. Besides the dependency of reddening on H $\alpha$  luminosity/surface brightness and gas phase metallicity, it is also correlated with the galaxy inclination, in the sense that edge-on galaxies are more attenuated than face-on galaxies at a given intrinsic luminosity. In light of these correlations, we present the empirical formulae of  $E(B - V)$  as a function of these galaxy properties, with a scatter of only 0.07 mag. The empirical relations can be reproduced if most dust attenuation to the H II region is due to diffuse interstellar dust distribution in a disc thicker than that of the H II region. The empirical formulae can be incorporated into semi-analytical models of galaxy formation and evolution to estimate the dust reddening and more practically enable comparison with observations.

**Key words:** dust, extinction – H II regions – galaxies: abundances – galaxies: ISM.

## 1 INTRODUCTION

Dust is a crucial component of galaxies in modifying the observed properties of galaxies by absorbing and scattering starlight, and also re-emits the absorbed energy in the mid- and far-infrared (hereafter mid-IR and far-IR respectively) bands. The extinction<sup>1</sup> cross-section of dust generally decreases with increasing wavelength, that is, the extinction is more severe at shorter wavelength, particularly at the ultraviolet (UV) band. As a result, the spectral energy distributions (SEDs) of galaxies appear redder, which is dubbed ‘reddening’. The effects of dust should be properly accounted for when interpreting the observations of the galaxies, for example, the luminosity or star formation rate (SFR) of a galaxy. For a galaxy with spectroscopic data covering suitable wavelengths, it is usually possible to estimate the amount of dust extinction from the spectrum. For example, the

average dust reddening of H II regions can be derived from the Balmer decrement, and be used to correct for the dust attenuation to the emission-line luminosity. In other cases, one has to rely on empirical relations to get an estimate of dust extinction in a statistical way.

Additionally, it is necessary to incorporate dust into the galaxy formation and evolution model. Currently, there are two ways to account for dust effects: full radiative transfer calculations assuming dust properties and geometric distribution; or adopting simple recipes obtained empirically. Since the dust formation in the galactic environment is a complicated chemical process, it has not yet been implemented in the current galaxy evolution models. The dust properties and distribution are input in the models and should be tested with observations. Alternatively, many authors have adopted the empirical relations to compute the perpendicular optical depth of a galactic disc, and then assign a random inclination angle for each galaxy to get the final dust corrections (e.g. Guiderdoni & Rocca-Volmerange 1987; Kauffmann et al. 1999; Somerville & Primack 1999; De Lucia, Kauffmann & White 2004; Kang et al. 2005; De Lucia & Blaizot 2007; Kitzbichler & White 2007). Therefore, a well-defined empirical recipe of dust reddening will help the comparison of model predictions with observations.

Previous studies have suggested that dust reddening in star-forming galaxies is correlated with the SFR, which can be well estimated with the intrinsic H $\alpha$  luminosity (e.g. Kennicutt 1998; Calzetti et al. 2010). Galaxies with large SFR (or high luminosity)

<sup>★</sup>E-mail: xiaoting@mail.ustc.edu.cn (TX); twang@ustc.edu.cn (TW)

<sup>1</sup>The nomenclature conventionally adopted is that: ‘extinction’ describes the absorption and scattering of light from a point source behind the dust screen; and the ‘attenuation’ describes the reduction and reddening of the light in a galaxy where stars and dust are mixed in geometrical distribution. In this work, we do not discriminate between these two terms when referring to the dust attenuation within the galaxy, except for the Galactic ‘extinction curve’ and the ‘attenuation curve’ for the starburst galaxies. The extinction and reddening can be converted to each other with an assumed extinction curve.

**Table 1.** Summary of sample-selection cuts.

Selection cut	Remaining number of galaxies	Per cent removed by the cut
SDSS DR5 spectroscopic sample	582 512	–
Photometric clean sample	495 165	14.99
S/N(H $\alpha$ ) > 20	191 289	61.37
S/N(H $\beta$ ) > 10	128 046	33.06
S/N([O III]) > 10	67 236	47.49
S/N([N II]) > 5	67 013	0.33
Removing broad-line AGN candidates	57 068	14.84
Removing multiple observations	56 241	1.45
Selecting star-forming galaxies using the BPT diagram	46 865	16.67
Requiring >20 per cent of the total light in the fibre	32 164	31.37
Selecting disc galaxies	23 919	25.63
Requiring $-2.5 < N2 < -0.4$	22 616	5.45

show strong global extinction in the emission lines (e.g. Wang & Heckman 1996; Charlot & Fall 2000; Calzetti 2001; Stasińska & Sodré 2001; Afonso et al. 2003; Kewley, Geller & Jansen 2004; Zoran, Barkana & Thompson 2006; Calzetti et al. 2007; Garn et al. 2010), and also large IR-to-UV flux ratios (e.g. Iglesias-Páramo et al. 2006, and reference therein).

In addition, it has been recognized that dust reddening might also be a function of gas-phase metallicity, that is, the reddening and extinction increase with metallicity. For instance, the average reddening to H $\alpha$  regions in an individual galaxy is correlated with the metallicity in the disc (e.g. Quillen & Yukita 2001; Boissier et al. 2004). For the case of whole galaxies, the relationship between reddening and metallicity also exists (e.g. Heckman et al. 1998; Buat et al. 2002; Asari et al. 2007). It is also supported by the fact that the low-metallicity galaxies such as blue compact galaxies are usually less reddened (e.g. Kong 2004).

Recently, Garn & Best (2010) also found a significant correlation between dust extinction and metallicity; however, they claimed that the dependency of reddening on stellar mass is more fundamental. They built a sample of about 90 000 star-forming galaxies using Sloan Digital Sky Survey (SDSS) data, and compared the relationship between the dust extinction of H $\alpha$  luminosity and SFR, metallicity as well as stellar mass. They concluded that the dust extinction  $A_{H\alpha}$  can be best predicted from the stellar mass, with a scatter of  $\sim 0.3$  mag.

Besides, the dependency of dust attenuation on inclination has been also investigated. While the correlation between the dust attenuation of optical stellar continua and disc inclination has been well established for disc galaxies (e.g. Driver et al. 2007; Shao et al. 2007; Unterborn & Ryden 2008), that of emission lines is still uncertain (e.g. Yip et al. 2010).

These works focused on how dust reddening depends on one property of galaxies, luminosity, metallicity or stellar mass, which are generally correlated with each other (e.g. Garnett & Shields 1987; Skillman, Kennicutt & Hodge 1989; Zaritsky, Kennicutt & Huchra 1994; Tremonti et al. 2004; Zahid, Kewley & Bresolin 2011). Disentangling the dependencies of dust reddening on these galaxy properties can not only help us to derive more accurate empirical formulae for dust reddening, but also provide more insight into the dust formation within the galactic environment. In this work, we study a large sample of star-forming disc galaxies in the local Universe with a median redshift of 0.07, selected from the spectroscopy data base of SDSS. We obtain empirical formulae for dust reddening as a function of intrinsic H $\alpha$  luminosity/surface brightness, gas-phase metallicity and the axial ratio of the disc.

In Section 2, we describe our sample selection, and in Section 3 we describe the spectral analysis and methods used to estimate the parameters such as the dust reddening, intrinsic H $\alpha$  luminosity, surface brightness, metallicity, axial ratio, etc. We present the resultant expression for the empirical formulae of dust reddening, and compare our results with previous work in Section 4. In Section 5, we reproduce the observed trend with a toy model of parallel-slab disc, which gives some insight into the geometry of dust distribution and dust-to-gas density ratio. Conclusions are given in Section 6. Throughout this paper, we will assume a cosmology of  $H_0 = 72 \text{ km s}^{-1} \text{ Mpc}^{-1}$ ,  $\Omega_M = 0.3$  and  $\Omega_\Lambda = 0.7$ .

## 2 DATA AND SAMPLE SELECTION

We start from the spectroscopic sample of galaxies in the Fifth Data Release of SDSS (DR5, Adelman-McCarthy et al. 2007). SDSS produces an imaging and spectroscopic survey with a wide-field 2.5-m telescope at the Apache Point Observatory, New Mexico (York et al. 2000). The survey provides imaging in five broad bands,  $u$ ,  $g$ ,  $r$ ,  $i$ ,  $z$ , with magnitude limits of 22.2 in the  $r$  band, and spectroscopic targets are selected using a variety of algorithms, including the ‘main’ sample of galaxies with  $r$ -band magnitude brighter than 17.77 (Strauss et al. 2002) with fibres of 3 arcsec diameter. The spectra range from 3200 to 9200 Å at a resolution  $R \equiv \lambda/\Delta\lambda = 1800$  (Adelman-McCarthy et al. 2007). The DR5 spectroscopic area covers 5740 deg $^2$ , and there are  $\sim 675 000$  spectra classified as galaxies. To select clean galaxies, we use the SDSS photometric flags to eliminate the targets that are only one part of a large galaxy or a part of merging galaxies. We list the sample-selection cuts and corresponding number of the remaining objects within each subsample in Table 1. Then, the galaxy spectra are corrected for Galactic extinction using a dust extinction map (Schlegel, Finkbeiner & Davis 1998) with an extinction curve of Fitzpatrick (1999) with  $R_V = 3.1$ .

We select emission-line galaxies where H $\alpha$  has been detected at high significance, that is, signal-to-noise ratio ( $S/N > 20$ ). To include galaxies of high reddening, we use a looser criterion on H $\beta$ :  $S/N > 10$ . The emission lines are measured with the procedures described in detail in Section 3.1. In order to use the ratios of [O III]/H $\beta$  and [N II]/H $\alpha$  in line-ratio diagnostic diagrams (e.g. BPT diagrams; Baldwin, Phillips & Terlevich 1981) for spectral classification, we also impose the criteria [O III]  $S/N > 10$  and [N II]  $S/N > 5$ . It should be noted that the requirement of lower limit in the  $S/N$  ratio for [N II] may drop some low-metallicity galaxies, and that for [O III] may miss high-metallicity galaxies. We will justify the  $S/N$  criteria in Section 4.2.

Galaxies with significant broad H $\alpha$  components are rejected. The broad-line active galactic nuclei (AGNs) are defined as objects for which adding an additional broad component of H $\alpha$  to the emission-line model can significantly improve the fit to the H $\alpha$ +[N II] blend (refer to Dong et al. 2005, 2007; also Zhou et al. 2006). In practice, the galaxies with broad H $\alpha$  components detected at the  $\geq 5\sigma$  significance level are regarded as candidates of broad-line AGNs, and removed from the sample. We also remove the narrow-line active galaxies by using the BPT diagram (Kauffmann et al. 2003b, hereafter Ka03; Kewley et al. 2006) based on the [N II]–H $\alpha$  diagram. The galaxies below the Ka03 pure star formation line in the [N II]–H $\alpha$  diagram are referred to as our sample of star-forming galaxies. Most of these galaxies lie below the extreme-starburst line in the [S II]–H $\alpha$  and [O I]–H $\alpha$  diagrams, with a fraction of 99 and 94 per cent, respectively. Using a more strict criterion on selecting H II galaxies, given by Stasińska et al. (2006), will result in less metal rich galaxies (see Section 3.3).

As shown by Kewley, Jansen & Geller (2005), if the nuclear spectrum contains less than 20 per cent of the total galaxy light, we will likely overestimate the global metallicity and reddening, and underestimate the global SFR by a significant fraction. Therefore, we remove the galaxies for which the fibre magnitude at the  $g$  band is greater than the total magnitude by 1.7 mag.

In the following analysis, we will pick out the late-type (presumably disc-dominated) galaxies from the star-forming galaxies based on the likelihoods provided by the SDSS pipeline. The photometry pipeline provides the likelihoods ( $\text{dev\_L}$ ,  $\text{exp\_L}$  and  $\text{star\_L}$ ) associated with the de Vaucouleurs, exponential and point spread function fits, respectively. The fractional likelihood for the exponential fit is calculated as

$$f(\text{exp\_L}) = \frac{\text{exp\_L}}{\text{exp\_L} + \text{dev\_L} + \text{star\_L}}, \quad (1)$$

and similarly for  $f(\text{exp\_L})$  and  $f(\text{star\_L})$ . It is suggested that fractional likelihood greater than 0.5 for any of the three model fits is generally good as a threshold for object classification (Stoughton et al. 2002). For a galaxy,  $f(\text{star\_L})$  is generally zero. We define a galaxy as a disc galaxy if the logarithmic likelihood for an exponential fit ( $r$  band) is larger than that of a de Vaucouleurs fit by 0.2 dex [corresponding to  $f(\text{exp\_L}) > 0.6$ ], and as an elliptical galaxy if the logarithmic likelihood for a de Vaucouleurs fit is larger than that of an exponential fit by 0.2 dex [ $f(\text{dev\_L}) > 0.6$ ]. This parameter is also correlated with the compactness index such as  $R_{50}/R_{90}$ , which is commonly used in quantitative classification (e.g. Shimasaku et al. 2001; Strateva et al. 2001). With this criterion, 23 919 star-forming galaxies are classified as disc galaxies, 7650 as elliptical galaxies, and 595 of unclassified type.

### 3 METHODS AND SAMPLE PROPERTIES

#### 3.1 Spectra analysis: starlight-continuum subtraction and emission-line fitting

In order to measure the emission lines, we take two steps to analyse the spectra: continuum fitting and emission-line fitting. First, we subtract the stellar continuum following the recipe described in Lu et al. (2006). In brief, Ensemble Learning for Independent Component Analysis has been applied to the simple stellar population library (Bruzual & Charlot 2003, hereafter BC03) to derive a set of templates, which are then shifted and broadened to match the stellar velocity dispersion of the galaxy, and reddened assuming a starburst-like extinction law to fit the observed galaxy spectra.

During the continuum fitting, the bad pixels flagged out by the SDSS pipeline as well as the emission-line regions are masked. From the fit, we obtain simultaneously the modelled stellar-light component, stellar velocity dispersion and an effective reddening<sup>2</sup> to the stellar light (refer to Lu et al. 2006, for details). Secondly, the emission lines are modelled with various Gaussians on the continuum-subtracted spectra, using the MPFIT package (Markwardt 2009)<sup>3</sup> implemented in Interactive Data Language (IDL). The formal  $1\sigma$  errors in flux obtained from the fitting are propagated from the error of the spectra, and then adopted as the emission-lines flux uncertainties. The emission lines we measure have been corrected for absorption lines, by subtracting the stellar component models. The typical absorption correction is 27 per cent of the flux of the H $\beta$  emission line. We examine the model fitting of higher order Balmer absorption lines, like H $\delta$ , which is less contaminated by emission lines, and estimate the uncertainty in absorption measurement to be less than 24 per cent, including the statistical uncertainty. Thus, the uncertainty in H $\beta$  absorption measurement is generally less than 6 per cent of H $\beta$  emission flux.

The corresponding emission-line regions are masked in the continuum fits. To determine the proper mask ranges for the emission lines, usually several iterations of the above procedures are required. Emission lines, H $\alpha$ , H $\beta$ , H $\gamma$ , H $\delta$ , He $\epsilon$ , [O II]  $\lambda\lambda 3727$  Å, [Ne III]  $\lambda\lambda 3869, 3969$  Å, [Ne V]  $\lambda 3427$  Å, [O III]  $\lambda 4363$  Å, He II  $\lambda 4686$  Å, [O III]  $\lambda\lambda 4959, 5007$  Å, [N I]  $\lambda 5199$  Å, He I  $\lambda 5876$  Å, [N II]  $\lambda\lambda 6548, 6584$  Å, [S II]  $\lambda\lambda 6716, 6731$  Å, [O I]  $\lambda\lambda 6300, 6344$  Å and [Ar III]  $\lambda 7136$  Å, are included in the first iteration, but insignificant ones (with  $S/N < 3$  in emission-line flux) are dropped in the later fitting. For robustness, we assume identical profiles for [N II] doublet lines and H $\alpha$ . The [S II] doublet lines are assumed to have the same profile and so are [O III] doublet lines. The ratios of [N II] doublets and [O III] doublets are fixed to their theoretical values, 2.96 and 3, respectively. The [O II] doublets are each modelled with a single Gaussian of the same width. To reduce the uncertainty in the measurements of weak emission lines, we fix their profiles to those of strong lines of similar ionization states. As the final procedure, upper limits are given to the undetected lines assuming that the lines have the same profile as the detected strong lines. If no emission line has been detected significantly ( $> 5\sigma$ ), no emission-line flux will be given for that spectrum.

#### 3.2 Reddening and $L_{H\alpha}$ correction

We estimate the reddening of emission lines using the Balmer decrement H $\alpha$ /H $\beta$  ratio. An intrinsic value of 2.86 as expected for case B recombination with electron density  $n_e = 100 \text{ cm}^{-3}$  at  $T = 10^4 \text{ K}$  is assumed (Osterbrock & Ferland 2006). This value is generally consistent with the lower limit of the measured H $\alpha$ /H $\beta$  ratio (Fig. 1a) in our sample. There is only a small fraction (about 1.5 per cent) of objects with the H $\alpha$ /H $\beta$  ratio below 2.86, likely due to measurement uncertainty. For these objects, the reddening is adopted as zero. Due to our stringent criteria for H $\beta$  and [O III] detections, a significant fraction of objects with high Balmer decrement values have been

<sup>2</sup> The effective reddening derived in this process is fairly well correlated with that of emission lines estimated using the Balmer decrements for H II galaxies (see also e.g. Calzetti, Kinney & Storchi-Bergmann 1994; Stasińska et al. 2004).

<sup>3</sup> The MPFIT package includes routines to perform non-linear least-squares curve fitting, kindly provided by Craig B. Markwardt, available at <http://purl.com/net/mpfit>.

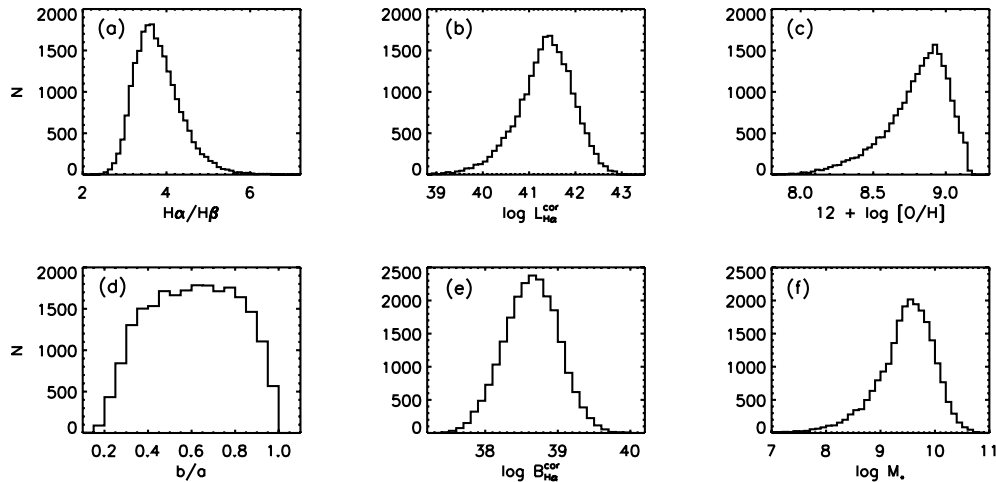


**Figure 1.** Distributions of properties for the selected  $\sim 22\,000$  disc-dominated H II galaxies from SDSS DR5 (see text): (a) Balmer decrement  $H\alpha/H\beta$ ; (b) dust-attenuation-corrected  $H\alpha$  luminosity  $\log L_{H\alpha}^{\text{cor}}$ ; (c)  $12 + \log (\text{O/H})$ ; (d) axial ratio  $b/a$ ; (e)  $H\alpha$  surface brightness corrected for dust attenuation  $\log B_{H\alpha}^{\text{cor}}$ , see equation (6); (f) stellar mass.

dropped; thus, most of our sample have  $H\alpha/H\beta < 7$ . The attenuation  $A_{H\alpha}$  is estimated from the Balmer decrement  $H\alpha/H\beta$  assuming an extinction curve, and then used to correct  $H\alpha$  luminosity.

We also apply aperture correction on  $H\alpha$  luminosity, based on the difference between the model magnitude and the fibre magnitude at the  $g$  band. This correction method assumes the distribution of  $H\alpha$  emission is the same as that of the stellar light (continuum emission). Such a correction is only an approximation because the line emission and the stellar continuum emission may not distribute in the same way. Some other authors use empirical approaches to make aperture corrections taking into account the colour differences within/outside the fibre (Brinchmann et al. 2004), or constrain the global SFR from fitting stochastic models to the photometric SED (Salim et al. 2007). The former method is based on the assumption that the distribution of specific SFR for a given set of colours inside the fibre is similar to that outside. We test with this method, but find that at a given set of colours the likelihood distribution of specific SFR inside the fibre varies with Balmer decrement. The typical specific SFR is higher for galaxies with larger Balmer decrement, and lower for galaxies with smaller Balmer decrement. Thus, this method of aperture correction may introduce dependence of  $H\alpha$  luminosity on Balmer decrement. Since our goal is to investigate the correlation between dust reddening and luminosity, we decide to settle for the simple scaling method. We also examine if the global SFR obtained with the method of Salim et al. (2007) is used, and compare with the SFR estimated from far-IR luminosity, as we will check for our corrected SFR in the following part of this section. The test suggests our simple method is no worse than theirs.

Because different parts of a galaxy suffer from different extinction, the extinction derived from the Balmer decrement is only a certain average. In the following, we will check if the aperture and attenuation correction introduce any fake correlation between  $H\alpha$  luminosity and reddening. If the corrected  $f(H\alpha)$  does not represent an accurate intrinsic  $H\alpha$  flux, then the SFR estimated from  $H\alpha$  luminosity will be inaccurate. To examine this issue, we use far-IR luminosity as the reference tracer for SFR and compare it with the SFR estimated from  $H\alpha$  luminosity. On one hand, although integrated IR emission should provide a robust measurement of SFR in dusty circumstances (Kennicutt 1998, and references therein; Dale & Helou 2002), there are also calibrations based on luminosities of

specific bands at the IR (e.g. Wu et al. 2005; Alonso-Herrero et al. 2006; Calzetti et al. 2007, 2010; Zhu et al. 2008; Rieke et al. 2009). At high luminosity ( $L_{70\,\mu\text{m}} \gtrsim 1.4 \times 10^{42} \text{ erg s}^{-1}$ ),  $L_{70\,\mu\text{m}}$  correlates linearly with SFR, thus could be used as a tracer of SFR (Calzetti et al. 2010, their equation 22):

$$\text{SFR}(70) (\text{M}_\odot \text{ yr}^{-1}) = 5.88 \times 10^{-44} L_{70\,\mu\text{m}}. \quad (2)$$

On the other hand, we adopt the calibration of Calzetti et al. (2010, their equation 5) to convert  $H\alpha$  luminosity to SFR as

$$\text{SFR}(H\alpha) (\text{M}_\odot \text{ yr}^{-1}) = 5.45 \times 10^{-42} L_{H\alpha} (\text{erg s}^{-1}), \quad (3)$$

in which  $L_{H\alpha}$  should be corrected for intrinsic extinction. This calibration is based on solar metallicity and the Kroupa (2001) initial mass function (IMF). The Kroupa IMF has two power laws, one with a slope of  $-1.3$  for stellar masses ranging from  $0.1$  to  $0.5 \text{ M}_\odot$  and the other with a slope of  $-2.3$  for stellar masses ranging from  $0.5$  to  $100 \text{ M}_\odot$ . This calibration is based on a  $t > 1$  Gyr age constant star formation stellar population.

We cross-match our parent sample of star-forming galaxies with the  $70\,\mu\text{m}$ -band photometry catalogues from the Spitzer Wide-area InfraRed Extragalactic Survey (SWIRE; Lonsdale et al. 2003) Data Release 3. To estimate the  $H\alpha$  SFR for the galaxies with confidence, we require the aperture to include at least 20 per cent of the total light (Kewley et al. 2005). We also require the detection of  $H\alpha$  emission to be more significant than  $10\sigma$ . In order to get a matched sample of reasonable size, we apply looser S/N criteria on other emission lines (i.e.  $\text{S/N} > 10$  for  $H\alpha$ , and  $\text{S/N} > 5$  for  $[\text{N}\,\text{II}]$ ,  $H\beta$  and  $[\text{O}\,\text{III}]$ ). With a matching radius of 5 arcsec, we get 156 star-forming galaxies with measurements of  $70\,\mu\text{m}$  fluxes. Removing five galaxies with contaminating sources nearby in IR emission, two galaxies with unreliable or problematic  $70\,\mu\text{m}$  fluxes, and one galaxy with problematic aperture correction (negative value), there are 148 galaxies left in the SWIRE star-forming galaxy sample.

We correct  $L_{H\alpha}$  for dust attenuation with three extinction curves: (i) the attenuation curve for the continuum of starburst galaxies (Calzetti et al. 2000); or (ii) the Galactic extinction curve of O'Donnell (1994); or (iii) the Galactic extinction curve of Fitzpatrick (1999). Converting  $L_{H\alpha}$  to SFR with equation (3), we investigate the ratio of  $\text{SFR}(H\alpha)/\text{SFR}(70)$  as a function of the Balmer decrement in the log-space. If  $L_{H\alpha}$  is properly corrected

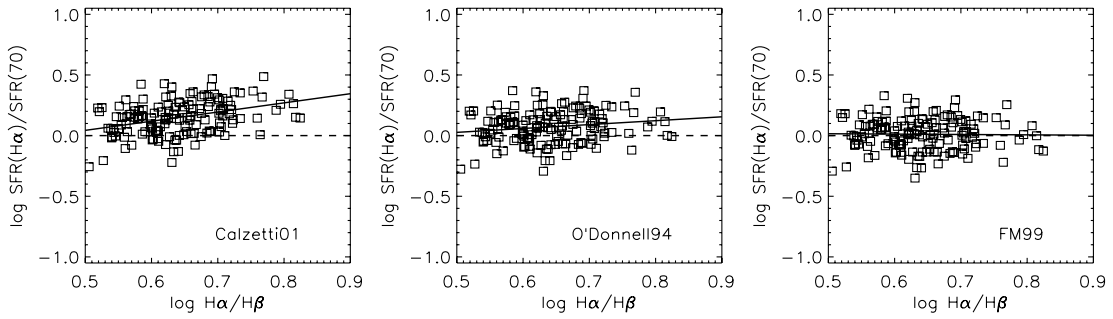


**Figure 2.** The ratio of  $SFR(H\alpha)/SFR(70)$  versus Balmer decrement  $H\alpha/H\beta$  in logarithmic scale.  $SFR(H\alpha) (M_\odot \text{ yr}^{-1}) = 5.45 \times 10^{-42} L_{H\alpha} (\text{erg s}^{-1})$ , where  $L_{H\alpha}$  is attenuation corrected with a starburst attenuation curve (Calzetti 2001, left-hand panel), or a Galactic extinction curve [middle panel: O'Donnell (1994) curve; right-hand panel: Fitzpatrick (1999) curve].  $SFR(70) (M_\odot \text{ yr}^{-1}) = 5.88 \times 10^{-44} L_{70 \mu\text{m}}$ . The solid lines represent the best fit for the sample, and the dashed lines represent  $SFR(H\alpha)/SFR(70) = 1$ .

for dust attenuation, the ratio of  $L_{H\alpha}/L_{70 \mu\text{m}}$ , thus the ratio of  $SFR(H\alpha)/SFR(70)$ , should be independent of the dust reddening and the Balmer decrement. In the SWIRE star-forming galaxy sample, there are 147 galaxies with  $L_{70 \mu\text{m}}$  greater than  $1.4 \times 10^{42} \text{ erg s}^{-1} \sim 3.7 \times 10^8 L_\odot$ , for which equation (2) can be used to estimate  $SFR(70)$ . Fig. 2 shows that if the starburst attenuation law is adopted (left-hand panel),  $SFR(H\alpha)/SFR(70)$  still correlates with  $H\alpha/H\beta$  (the Spearman rank coefficient  $r_s = 0.33$ , with the probability of null hypothesis  $P_{\text{null}} < 10^{-4}$ ), implying that  $L_{H\alpha}$  might have been overcorrected than demanded, while the Galactic extinction curves give better correction on average (middle and right-hand panels). With the Fitzpatrick (1999) curve, the ratio  $SFR(H\alpha)/SFR(70)$  is uncorrelated to the Balmer decrement ( $r_s = -0.01, P_{\text{null}} = 0.90$ ). This means the  $H\alpha$  SFR can be well determined from the attenuation-corrected  $L_{H\alpha}$  by assuming Fitzpatrick's curve. Therefore, we will adopt this curve for attenuation correction to  $L_{H\alpha}$  in the following analysis.

For our final sample of star-forming disc galaxies, the corrected  $L_{H\alpha}$  is shown in a distribution histogram in Fig. 1(b). The dust-extinction-corrected  $H\alpha$  luminosity is in the range  $4 \times 10^{37} - 2 \times 10^{43} \text{ erg s}^{-1}$ , with a median value of  $3 \times 10^{41} \text{ erg s}^{-1}$ . The typical error in  $L_{H\alpha}$  is 0.04 dex, as the quadrature sum of the measurement uncertainty in observed flux of  $H\alpha$  emission, and the Balmer decrement used for attenuation correction. The uncertainty induced by either the average reddening we simply assumed or the aperture correction for  $L_{H\alpha}$  has not been included. Assuming Fitzpatrick's extinction curve, the colour excess is estimated as

$$\begin{aligned} E(B-V) &= 1.99 \log_{2.86} \frac{H\alpha/H\beta}{2.86} && \text{for } H\alpha/H\beta \geq 2.86 \\ &= 0 && \text{for } H\alpha/H\beta < 2.86. \end{aligned} \quad (4)$$

The median formal uncertainty in the  $H\alpha/H\beta$  ratio for our selected sample is typically 3.4 per cent, which gives an uncertainty of 0.03 mag in  $E(B-V)$ . The uncertainty of  $E(B-V)$  is about 0.04 mag typically for the small sample of SWIRE star-forming galaxies. We also calculate  $E(B-V)$  from the ratio of  $H\alpha/H\gamma$  assuming Fitzpatrick's extinction curve, and the derived  $E(B-V)$  is quite consistent with the value obtained using equation (4). This proves that our corrections for Balmer absorption are quite robust.

We note that in the relation between  $SFR(H\alpha)/SFR(70)$  and Balmer decrement, irrespective of which extinction curve is adopted, there is a moderate scatter  $\sim 0.13$  dex. This scatter includes the measurement errors of observed  $L_{H\alpha}$ ; the Balmer decrement and model/fibre magnitudes at the  $g$  band; the uncertainty in aperture correction and attenuation correction; the measurement error in observed  $L_{70 \mu\text{m}}$ ; and the calibration error in the  $SFR(H\alpha)/SFR(70)$

ratio. The overall measurement error for  $SFR(H\alpha)$  is typically 0.04 dex, and for  $SFR(70)$  typically 0.01 dex. Then, the remaining scatter of 0.12 dex accounts for the sum in quadrature of uncertainties in aperture and attenuation correction, and the calibration scatter in  $SFR(H\alpha)/SFR(70)$ . Therefore, any one of these uncertainties, for example, the calibration scatter in  $SFR(H\alpha)/SFR(70)$  should be less than 0.12 dex, which is smaller than the calibration uncertainty in  $SFR(70)$  of equation (2),  $\sim 0.2$  dex (Calzetti et al. 2010, refer to their Section 5). Note in passing, we obtained a larger scatter ( $\sim 0.17$  dex) in  $SFR(H\alpha)/SFR(70)$  if the  $SFR(H\alpha)$  from the MPA-JHU<sup>4</sup> catalogue (Brinchmann et al. 2004) is used instead.

### 3.3 Metallicity

Estimating global metallicity has been widely studied by using strong lines. However, there is still no consensus on which line ratio should be used. Ratios of strong lines, such as  $R_{23} \equiv \log([O\text{II}] \lambda 3727 \text{ \AA} + [O\text{III}] \lambda\lambda 4959, 5007 \text{ \AA})/H\beta$ ,  $[N\text{II}] \lambda 6584 \text{ \AA}/[O\text{II}] \lambda 3727 \text{ \AA}$ ,  $N2 \equiv \log([N\text{II}] \lambda 6584 \text{ \AA}/H\alpha)$ , and  $O3N2 \equiv \log([O\text{III}] \lambda 5007 \text{ \AA}/H\beta)/([N\text{II}] \lambda 6584 \text{ \AA}/H\alpha)$  are used to estimate the oxygen abundance (e.g. McGaugh 1991; Storchi-Bergmann, Calzetti & Kinney 1994; Denicoló, Terlevich & Terlevich 2002; Kewley & Dopita 2002; Pilyugin 2003; Pettini & Pagel 2004, hereafter PP04; Tremonti et al. 2004; Pilyugin & Thuan 2005; Liang et al. 2006; Nagao, Maiolino & Marconi 2006; Shi, Kong & Cheng 2006). The commonly used metallicity indicator  $R_{23}$  is not used here, because it includes  $[O\text{II}]$  emission line which is much prone to dust extinction. Note that one purpose of our work is to investigate the relation between dust reddening and metallicity, so we should avoid any spurious correlation potentially caused by reddening correction. The estimators  $N2$  and  $O3N2$  are both not sensitive to reddening correction. However, the measurement error of  $O3N2$  (typically 0.03 dex) is larger than that of  $N2$  (typically 0.01 dex). Therefore,  $N2$  is preferred as our metallicity diagnostic.

The relation of line ratio versus abundance can be generally calibrated using two different approaches: (i) the empirical method relying on the electron temperature  $T_e$  as a surrogate for metallicity (cooling increases with metallicity); or (ii) a comparison with photoionization models. Note that different methods lead to systematic differences in the calibrated relations up to a factor of 3 or more in some extreme cases, apart from the limited range for the

<sup>4</sup> The MPA-JHU catalogue and the total SFRs are provided on the website: <http://www.mpa-garching.mpg.de/SDSS/DR7/>.

validation of the relations (refer to Kewley & Ellison 2008, for a detailed discussion).

We estimate the metal abundance with the  $N2$  index of PP04, further revised by Nagao et al. (2006) and Liang et al. (2006). PP04 derived their empirical relationships between line ratios and  $T_e$ -based metallicities for H II regions, while Nagao et al. and Liang et al. calibrated various line ratios to the metallicities obtained with theoretical methods based on photoionization model fits by Tremonti et al. (2004). The three calibrations yield very similar estimates of [O/H] at low abundances [e.g.  $12 + \log(\text{O/H}) < 8.5$ ], but they deviate considerably at high abundances [e.g.  $12 + \log(\text{O/H}) > 8.5$ ]: PP04 give a lower abundance value than those of Liang et al. (2006) and Nagao et al. (2006). Since PP04 calibration does not extend to high abundances [most of their objects have  $7.5 < 12 + \log(\text{O/H}) < 8.5$ ], we adopt the calibration of Nagao et al. (2006), expressed as

$$N2 = 96.641 - 39.941 \times y + 5.2227 \times y^2 - 0.22040 \times y^3, \quad (5)$$

where  $y \equiv 12 + \log(\text{O/H})$ . Equation (5) is valid within the metallicity range  $7.15 \leq 12 + \log(\text{O/H}) \leq 9.16$ , corresponding to  $-2.5 \leq N2 \leq -0.4$ .<sup>5</sup> We estimate the metallicity for our sample with  $N2$  for consistency; thus, we reject those objects with  $N2 > -0.4$  (only about 5 per cent in our sample). Note that this selection has little effect on the results we obtain in this paper. The final sample consists of 22 616 galaxies, with the oxygen abundance in the range of  $7.64 < 12 + \log(\text{O/H}) < 9.16$  and with a median value  $\langle 12 + \log(\text{O/H}) \rangle = 8.84$  (Fig. 1c). The oxygen abundances could be converted to metallicity in units of solar metallicity ( $Z_\odot = 0.02$ ), adopting a value of  $12 + \log(\text{O/H})_\odot = 8.66$  (Asplund et al. 2004), and the range is  $0.1 < Z/Z_\odot < 3.2$ , with a median of  $\langle Z/Z_\odot \rangle = 1.5$ .

The error in the metallicity includes measurement uncertainty and calibration uncertainty. For our sample, the metallicity is estimated using  $N2$ , and the typical measurement uncertainty in  $N2$  is 2.5 per cent, which corresponds only up to 0.02 dex in  $12 + \log(\text{O/H})$ . The main uncertainty in metallicity estimation comes from the scatter of the calibration of the  $N2$  indicator. Nagao et al. did not explicitly provide the scatter of their calibration (equation 5). However, PP04 proposed a linear calibration of  $N2$  and indicated the  $1\sigma$  uncertainty in  $Z$  is 0.18 dex. The  $N2$  calibration in equation (5) differs significantly ( $\Delta Z \geq 0.2$  dex) from PP04's calibration only at metallicities  $12 + \log(\text{O/H}) < 7.5$  and  $12 + \log(\text{O/H}) > 8.5$ . Moreover, Kewley & Ellison (2008) compared various metallicity calibrations, and concluded that metallicities estimated from strong-line methods should be consistent within 0.15 dex. Therefore, we estimate the upper limit of the uncertainty in metallicity to be  $\Delta Z \sim 0.15$  dex.

### 3.4 Surface brightness $B_{\text{H}\alpha}$ , disc inclination and other properties

The surface brightness of a galaxy is the flux received from a unit solid angle as it appears on the sky; then, we define the intrinsic surface brightness  $B_{\text{H}\alpha}$  as the  $\text{H}\alpha$  luminosity per unit area within the half-light radius of the galaxy, that is,

$$B_{\text{H}\alpha} \equiv \frac{L_{\text{H}\alpha}}{8\pi^2 R_{50}^2} \quad (\text{erg s}^{-1} \text{kpc}^{-2}), \quad (6)$$

<sup>5</sup> Nagao et al. (2006) did not specify the valid range of  $N2$  for their calibration; we adopt the range of their observational sample used for calibration. We are prudent to not use the extrapolation when  $N2 > -0.4$ , which saturates and yields quite high and unreasonable metallicities.

where  $R_{50}$  is the Petrosian half-light physical radius (in kpc) in the  $r$  band, which can be obtained by the product of the Petrosian half-light radius (in arcsec) provided by the SDSS pipeline and angular distance. The apparent surface brightness is dimmer than  $B_{\text{H}\alpha}$  with redshift by a factor of  $(1+z)^{-4}$ . The distribution of  $B_{\text{H}\alpha}$  is shown on Fig. 1(e), and the formal uncertainty for  $B_{\text{H}\alpha}$  is about 0.05 dex. We will use this definition of  $B_{\text{H}\alpha}$  to compare with a toy model in the next section. We use the axial ratio in the exponential fit of the galaxy ( $\text{AB}_{\text{exp}}$  given by the SDSS pipeline) as a surrogate for the disc inclination (Fig. 1d). While the axial ratio  $b/a$  close to 1 means that the disc galaxy is face-on,  $b/a$  close to 0 means the disc is edge-on. The typical error of  $b/a$  is about 0.02. Note that Petrosian radius is defined as the radius at which the ratio of the averaged surface brightness in a local annulus to the mean surface brightness within it equals to some specified value (0.2 for SDSS; Blanton et al. 2001; Yasuda et al. 2001). Thus, Petrosian radius is not very sensitive to disc inclination. However, the  $\text{H}\alpha$  surface brightness  $B_{\text{H}\alpha}$  estimated in equation (6) is only a crude average approximation, because H II regions likely occupy only a portion of the galaxy, and the distribution may be very inhomogeneous.

The stellar mass  $M_*$  (Fig. 1f) is calculated from template fits to the SDSS five-band photometry with the KCORECT package (Blanton & Roweis 2007) in IDL. The magnitudes are corrected to the AB system ( $-0.036, 0.012, 0.010, 0.028$  and  $0.040$  for the  $ugriz$  filters, respectively) and corrected for Galactic extinction. In short, Blanton & Roweis (2007) built their five templates using a technique of non-negative matrix factorization based on a set of 450 instantaneous burst stellar population models (Bruzual & Charlot 2003) and 35 emission templates of MAPPINGS III models (Kewley et al. 2001). Specifically, the stellar population models include all six metallicities ( $Z$  from 0.0001 to 0.05) and 25 ages (from 1 Myr to 13.75 Gyr) based on the Chabrier (2003) stellar IMF and the Padova 1994 isochrones (Fagotto et al. 1994a,b). For each stellar population model, three different dust models are assumed: (i) no dust extinction; (ii)  $\tau_V = 3$  with Milky Way like extinction; or (iii)  $\tau_V = 3$  with Small Magellanic Cloud like extinction. They assumed a homogeneous dust distribution and shell geometry for the latter two dust models. The authors compared their measurements of stellar masses for SDSS galaxies with those obtained by Kauffmann et al. (2003a), and found that the two sets of masses are consistent with each other, with a scatter of only 0.1 dex (refer to their fig. 17 in Blanton & Roweis 2007).

In addition to these parameters, we also look into other properties based on the spectra. The 4000-Å discontinuity is due to the opacity from ionized metals, and its amplitude indicates the stellar population ages. In hot stars, the metal elements are multiply ionized and the opacity decreases; thus, the 4000 Å break strength is small for young stellar populations and large for old, metal-rich populations (Bruzual 1983; Balogh et al. 1999). The break discontinuity is generally defined as the ratio of the continua redwards and bluewards of 4000 Å. We adopt the narrow definition  $D_n(4000)$  introduced by Balogh et al. (1999) using the bands 3850–3950 Å and 4000–4100 Å.  $D_n(4000)$  is measured from the reddening-corrected modelled spectrum, which is obtained in the continuum fits described in Section 3.1, instead of directly from the observed spectrum. An extensive test shows that the former has two advantages over the latter. One is that for the observed spectrum of low S/N, the model fitting provides a filter to the noises on the observed spectrum. The other is, on the modelled spectrum, the bias in  $D_n(4000)$  introduced by reddening can be corrected, about an offset of 0.03 larger for the typical reddening [ $E(B-V) = 0.23$ ] of our sample. H $\delta$  absorption line equivalent width (EW), which reaches a peak for the

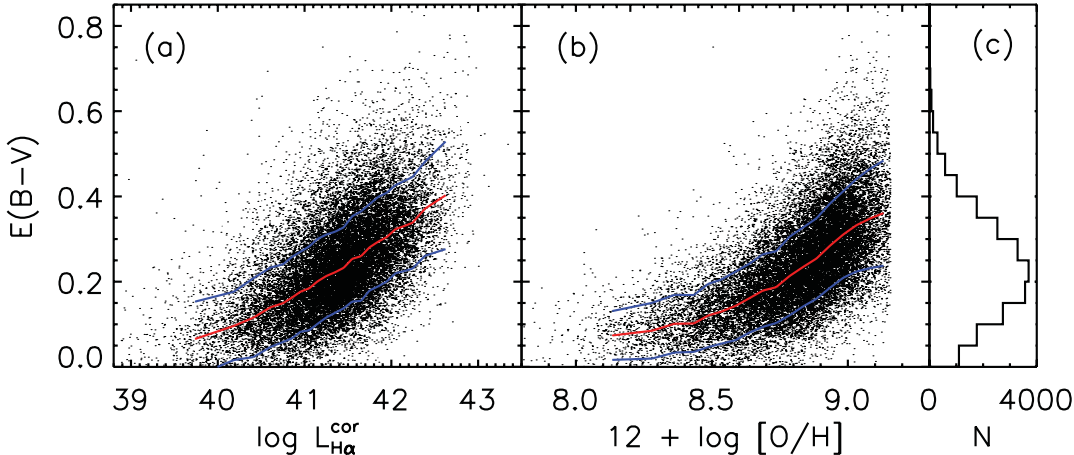


**Figure 3.** The reddening of emission lines parametrized by  $E(B - V)$  as a function of (a) attenuation-corrected  $\text{H}\alpha$  luminosity  $L_{\text{H}\alpha}$  (in units of  $\text{erg s}^{-1}$ ) and (b) oxygen abundance for our final sample of 22 616 star-forming disc-dominated galaxies. The red line is the median value, while the blue lines enclose 68 per cent ( $1\sigma$ ) of the objects at a given  $\log L_{\text{H}\alpha}^{\text{cor}}$  or  $12 + \log (\text{O}/\text{H})$ . (c) Distribution of  $E(B - V)$ .

stellar population of age  $\sim 0.1\text{--}1$  Gyr (the Lick index  $\text{H}8_A$ , Worthey & Ottaviani 1997; Kauffmann et al. 2003a), is measured from the modelled continuum as well. The electron density is estimated from the ratio of  $[\text{S II}] \lambda\lambda 6716, 6731 \text{ \AA}$  (Osterbrock & Ferland 2006).

#### 4 RELATION BETWEEN INTRINSIC REDDENING AND OTHER GALAXY PROPERTIES

In this section, we will investigate the correlations between intrinsic dust reddening and other observable properties or those properties that could be deduced from observations. The properties include the gas metallicity, the attenuation-corrected  $\text{H}\alpha$  luminosity or surface brightness, stellar mass, and the inclination of the disc.

For the  $\sim 22\,000$  star-forming disc-dominated galaxies in our final sample, the distributions of emission-line reddening, which is parametrized by  $E(B - V)$ , are shown as a function of  $L_{\text{H}\alpha}$  (Fig. 3a) or  $12 + \log (\text{O}/\text{H})$  (Fig. 3b). In Fig. 3(b), the metallicity estimated from  $N2$  has a cut-off at  $12 + \log (\text{O}/\text{H}) = 9.16$ , which corresponds to  $N2 = -0.4$ . The histogram of  $E(B - V)$  distribution is shown in Fig. 3(c). While the  $E(B - V)$  range is wide ( $0.0\text{--}1.0$  mag), 95 per cent of our sample is in the range  $0.05\text{--}0.6$  mag.

Fig. 3 shows that the reddening increases both with increasing  $L_{\text{H}\alpha}$  and with increasing  $12 + \log (\text{O}/\text{H})$ . The intrinsic dust reddening is clearly correlated with the  $\text{H}\alpha$  luminosity, with a Spearman rank coefficient  $r_s = 0.59$  ( $P_{\text{null}} < 10^{-5}$ ) for our sample of star-forming disc galaxies (Fig. 3a). This relation has been known for a long time (e.g. Wang & Heckman 1996; Calzetti 2001; Hopkins et al. 2001; Afonso et al. 2003). The reddening correlates with  $\text{H}\alpha$  surface brightness as well (not shown in the figure), with  $r_s = 0.51$  ( $P_{\text{null}} < 10^{-5}$ ). On the other hand, the reddening is also correlated with the gas-phase metallicity indicated by oxygen abundance  $12 + \log (\text{O}/\text{H})$  ( $r_s = 0.67$ ,  $P_{\text{null}} < 10^{-5}$ , Fig. 3b), which has also been known previously (e.g. Heckman et al. 1998; Boissier et al. 2004; Asari et al. 2007). At low metallicity, the reddening increases slowly with  $[\text{O}/\text{H}]$ , but at high metallicity, it rises more sharply. The correlation between  $E(B - V)$  and metallicity is the strongest among all the correlations; therefore, we divide our sample into bins of metallicity to investigate the relations of reddening with other parameters ( $\text{H}\alpha$  luminosity/surface brightness, axial ratio, stellar mass, etc.) at a given metallicity bin in the rest part of this section.

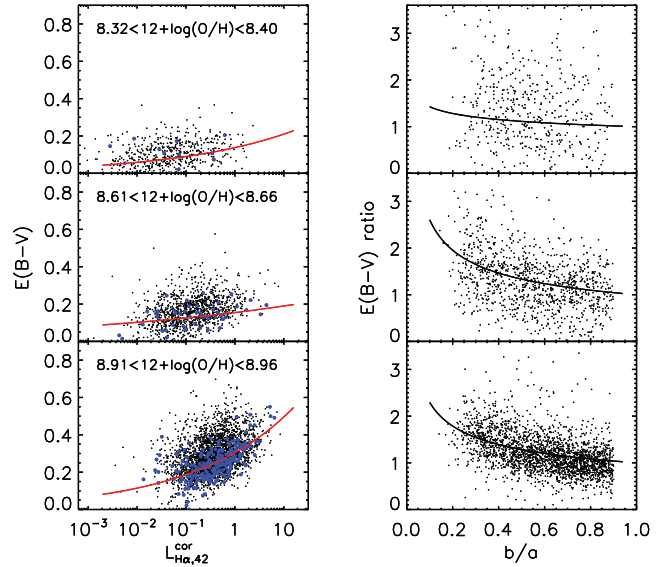


**Figure 4.** Left-hand column:  $\log L_{\text{H}\alpha}$  versus  $E(B - V)$ .  $L_{\text{H}\alpha}$  is in units of  $\text{erg s}^{-1}$ . The black dots represent the galaxies with axial ratio  $b/a < 0.9$ , and the blue dots represent the face-on galaxies ( $b/a > 0.9$ ). The red lines are the best-fitting power law for face-on galaxies in each metallicity bin. Right-hand column: the  $E(B - V)$  ratio versus the axial ratio  $b/a$  for each metallicity bin. The  $E(B - V)$  ratio is the ratio of  $E(B - V)$  in other galaxies to that deduced from the best-fitting power law of  $L_{\text{H}\alpha}$  for face-on galaxies. The solid line presents the best fit. The three metallicity bins are  $0.5, 1$  and  $2 Z_{\odot}$ , as marked in the left-hand column.

We divide the sample into continuous metallicity bins. The bin is so chosen that a bin size is no less than 0.05 in  $12 + \log (\text{O}/\text{H})$ , with at least 400 objects in each bin. In order to isolate inclination dependence, we check the relation between  $E(B - V)$  and  $L_{\text{H}\alpha}$  for nearly-face-on galaxies, that is,  $(b/a) > 0.90$ , and then compare it with the rest of the galaxies. Clearly, face-on galaxies have systematically small  $E(B - V)$  values than the others at a given intrinsic  $L_{\text{H}\alpha}$  (Fig. 4, left-hand column). We fit the relation of reddening with luminosity for these face-on galaxies using a power-law function. For a galaxy, the  $E(B - V)$  ratio is defined as the ratio of  $E(B - V)$  of this galaxy to the expected  $E(B - V)$  based on its  $\text{H}\alpha$  luminosity from the best-fitting power-law function for the face-on

**Table 2.** Coefficients of empirical fits to reddening in a function such as equation (7).<sup>a</sup>

Metallicity bin	Number of galaxies	$p$	$q$	$\gamma$	$\chi^2_v$
$12 + \log(\text{O/H}) < 8.22$	423	$0.104 \pm 0.003$	$0.132 \pm 0.006$	$-0.196 \pm 0.027$	10.75
$8.22 < 12 + \log(\text{O/H}) < 8.32$	448	$0.106 \pm 0.003$	$0.083 \pm 0.007$	$-0.060 \pm 0.029$	9.14
$8.32 < 12 + \log(\text{O/H}) < 8.40$	515	$0.135 \pm 0.003$	$0.159 \pm 0.007$	$-0.155 \pm 0.027$	7.01
$8.40 < 12 + \log(\text{O/H}) < 8.46$	539	$0.139 \pm 0.003$	$0.108 \pm 0.006$	$-0.054 \pm 0.023$	7.41
$8.46 < 12 + \log(\text{O/H}) < 8.51$	568	$0.138 \pm 0.002$	$0.128 \pm 0.005$	$-0.260 \pm 0.020$	5.84
$8.51 < 12 + \log(\text{O/H}) < 8.56$	733	$0.150 \pm 0.002$	$0.138 \pm 0.005$	$-0.284 \pm 0.018$	6.65
$8.56 < 12 + \log(\text{O/H}) < 8.61$	819	$0.162 \pm 0.002$	$0.159 \pm 0.004$	$-0.292 \pm 0.014$	7.26
$8.61 < 12 + \log(\text{O/H}) < 8.66$	1088	$0.158 \pm 0.002$	$0.141 \pm 0.004$	$-0.416 \pm 0.012$	6.20
$8.66 < 12 + \log(\text{O/H}) < 8.71$	1329	$0.188 \pm 0.002$	$0.166 \pm 0.003$	$-0.380 \pm 0.010$	6.51
$8.71 < 12 + \log(\text{O/H}) < 8.76$	1583	$0.195 \pm 0.001$	$0.171 \pm 0.003$	$-0.418 \pm 0.009$	6.09
$8.76 < 12 + \log(\text{O/H}) < 8.81$	1917	$0.212 \pm 0.001$	$0.165 \pm 0.003$	$-0.433 \pm 0.008$	7.09
$8.81 < 12 + \log(\text{O/H}) < 8.86$	2162	$0.231 \pm 0.001$	$0.162 \pm 0.002$	$-0.391 \pm 0.006$	6.97
$8.86 < 12 + \log(\text{O/H}) < 8.91$	2456	$0.241 \pm 0.001$	$0.143 \pm 0.002$	$-0.438 \pm 0.006$	7.02
$8.91 < 12 + \log(\text{O/H}) < 8.96$	2551	$0.279 \pm 0.001$	$0.152 \pm 0.002$	$-0.361 \pm 0.005$	8.27
$8.96 < 12 + \log(\text{O/H}) < 9.01$	2191	$0.299 \pm 0.001$	$0.139 \pm 0.002$	$-0.338 \pm 0.005$	8.97
$9.01 < 12 + \log(\text{O/H}) < 9.06$	1652	$0.315 \pm 0.001$	$0.144 \pm 0.002$	$-0.368 \pm 0.006$	10.64
$9.06 < 12 + \log(\text{O/H}) < 9.11$	1052	$0.321 \pm 0.001$	$0.154 \pm 0.002$	$-0.397 \pm 0.007$	13.53
$12 + \log(\text{O/H}) > 9.11$	590	$0.318 \pm 0.002$	$0.166 \pm 0.003$	$-0.430 \pm 0.009$	11.33

<sup>a</sup>Empirical relation of reddening parametrized by colour excess  $E(B - V)$ , as a function of  $L_{\text{H}\alpha}$  and axial ratio  $b/a$  in different metallicity bins.

galaxies. The  $E(B - V)$  ratio is found to correlate with the axial ratio, which can be well fitted by  $(b/a)^\gamma$ . Fig. 4 shows  $\log L_{\text{H}\alpha}$  versus  $E(B - V)$  as well as the best-fitting curve for the face-on objects in the left-hand column, and the dependency of the  $E(B - V)$  ratio on the axial ratio  $b/a$  in the right-hand column. These results are only illustrated for three metallicity bins:  $12 + \log(\text{O/H}) \simeq 8.36$ , 8.64 and 8.94 (i.e.  $\sim 0.5$ , 1 and  $2 Z_\odot$ , respectively, adopting  $[12 + \log(\text{O/H})]_\odot = 8.66 \pm 0.05$ , Asplund et al. 2004). The correlation between the  $E(B - V)$  ratio and the axial ratio becomes stronger as the metallicity increases, for example,  $r_s = -0.49$  ( $P_{\text{null}} < 10^{-5}$ ) for the bottom metallicity bin,  $12 + \log(\text{O/H}) \simeq 8.94$ . We fit the data in each bin with a joint function in the form of

$$E(B - V) = p L_{\text{H}\alpha, 42}^q (b/a)^\gamma, \quad (7)$$

where  $L_{\text{H}\alpha, 42} \equiv L_{\text{H}\alpha}/(10^{42} \text{ erg s}^{-1})$ . For each metallicity bin, the fitting parameters are obtained by minimizing  $\chi^2$  in the fitting implemented by MPFIT, and the results are listed in Table 2. Only uncertainties in  $E(B - V)$  have been considered in the fitting; thus, the errors of the fitting parameters are underestimated.

Fig. 5 shows  $p$ ,  $q$  and  $\gamma$  as a function of metallicity. We can see that  $p$  increases with metallicity, and can be fitted with an exponential function of  $12 + \log(\text{O/H})$ , that is, a power-law function of metallicity  $Z$ , in the form of

$$\begin{aligned} p &= (0.072 \pm 0.001) \exp\left(\frac{x}{0.71 \pm 0.01}\right) \\ &= (0.18 \pm 0.02) \left(\frac{Z}{Z_\odot}\right)^{0.61 \pm 0.01}, \end{aligned} \quad (8)$$

where  $x = 12 + \log(\text{O/H}) - 8$ . The power-law index  $q$  varies slightly between 0.08 and 0.17, and the average value is about 0.15. We therefore adopt the parameter  $q$  as a constant:

$$\langle q \rangle = 0.15. \quad (9)$$

$|\gamma|$  first increases from about 0.1 with metallicity and then reaches to a constant ( $|\gamma| \sim 0.4$ ) at about  $12 + \log(\text{O/H}) \simeq 8.5$ . We use a step function to fit  $\gamma$  as a function of  $12 + \log(\text{O/H})$ , which is

expressed as

$$\begin{aligned} \gamma &= -0.1 && \text{for } 0.1 < x < 0.5 \\ &= -0.4 && \text{for } 0.5 \leq x < 1.2. \end{aligned} \quad (10)$$

Substituting  $p$ ,  $q$  and  $\gamma$  into equation (7), we will get the overall function of luminosity, metallicity and inclination, and we call this  $(L_{\text{H}\alpha}, Z, b/a)$  model hereafter. To verify the reliability of our empirical formulae, we define the  $E(B - V)$  residual as  $\Delta E(B - V) \equiv E(B - V)_{\text{obs}} - E(B - V)_{\text{model}}$ , and show its distribution in Fig. 6 (first column, upper panel). The  $E(B - V)$  distribution can be well fitted with a Gaussian profile, with width  $\sigma = 0.068$  mag. If we adopt a more stringent S/N criterion ( $S/N > 100$ ) on  $\text{H}\alpha$  emission, the result will yield a sample of  $\sim 5000$  star-forming disc galaxies. We repeat the procedure above and find the scatter of  $\Delta E(B - V)$  remains similar,  $\sigma = 0.066$  mag, indicating that the scatter is independent of  $\text{H}\alpha$  S/N, in the S/N range we considered (we will discuss in more detail and show that our S/N criterion is reasonable in Section 4.2). Besides, we find that  $\Delta E(B - V)$  is uncorrelated with the parameters including  $L_{\text{H}\alpha}$ , metallicity or axial ratio (Fig. 6, three right-hand side columns), which suggests that the  $(L_{\text{H}\alpha}, Z, b/a)$  model considered above reproduces the intrinsic reddening well in the disc galaxies.

Note that at low metallicities the scatter in the relation between  $E(B - V)$  ratio and  $b/a$  is larger than that at high metallicities (Fig. 5, right-hand column). The power-law index  $\gamma$  is close to zero at low metallicity, that is, the relationship between  $E(B - V)$  ratio and  $b/a$  is almost flat, while  $\gamma \sim -0.4$  when the metallicity increases to a solar or supersolar value. This suggests that dust reddening is not as sensitive to the axial ratio at low metallicity as at high metallicity. It may be attributed to two possible reasons. One is that the relation at low metallicity might remain as strong as at high metallicity, but the limited dynamic range of  $E(B - V)$  and the measurement uncertainties prevent us from recovering the relationship. The  $E(B - V)$  dynamic range is only about 0.2 mag at low metallicity, and increases to 0.8 mag at high metallicity. The other possible reason is that the relation indeed becomes weaker at low metallicity. At present we cannot decide which one is true, especially when the number of face-on galaxies at low metallicity is

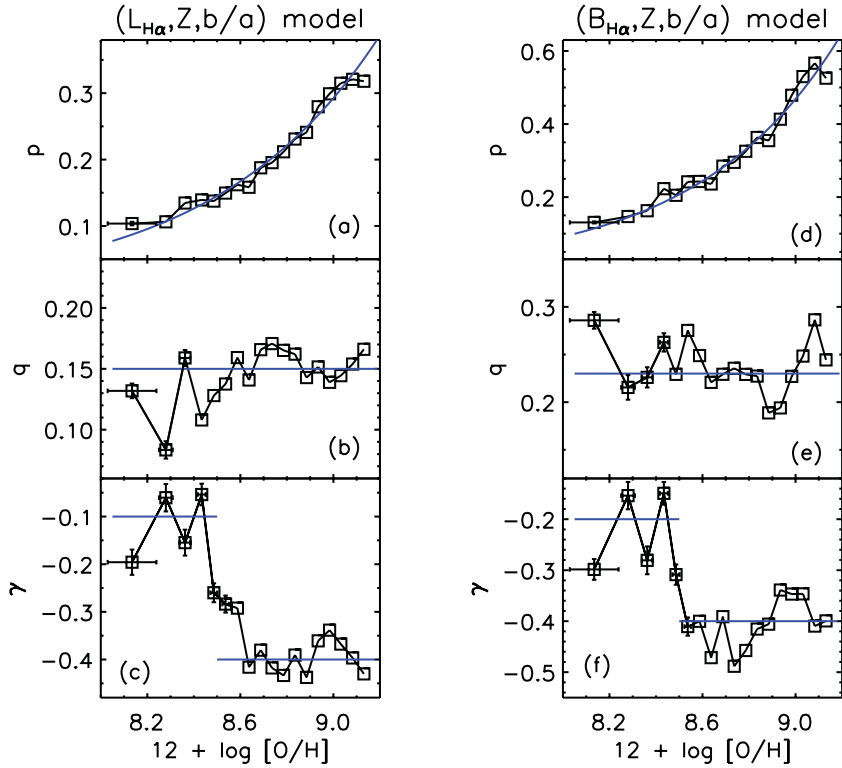


**Figure 5.** Fitting parameters as a function of metallicity. (a)  $p$ , (b)  $q$  and (c)  $\gamma$  are from equation (7), and (d)  $p$ , (e)  $q$  and (f)  $\gamma$  are from equation (11). Those symbols without error bars indicate the error is smaller than the symbol size. In each panel, the best-fitting function is shown in the blue solid line.

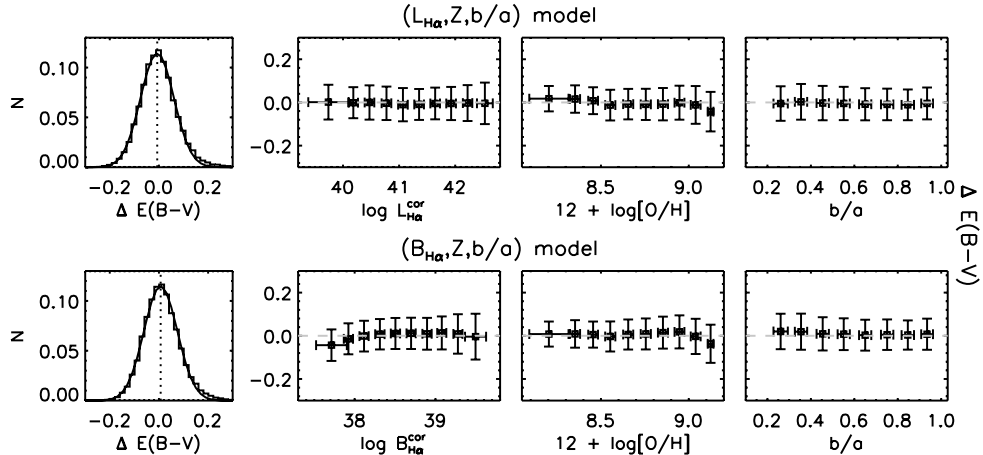


**Figure 6.** The first column shows the distribution of  $E(B - V)$  residuals in our sample for the two empirical models: the  $(L_{H\alpha}, Z, b/a)$  model and the  $(B_{H\alpha}, Z, b/a)$  model.  $\Delta E(B - V)$  is defined as  $\Delta E(B - V) \equiv E(B - V)_{\text{obs}} - E(B - V)_{\text{model}}$ .  $N$  is the fraction of the total sample. The best-fitting Gaussian is overplotted with the centre shown in the dotted line for each model. The second to fourth columns show  $\Delta E(B - V)$  as a function of  $L_{H\alpha}$  or  $B_{H\alpha}$  (in units of  $\log \text{erg s}^{-1}$  or  $\text{erg s}^{-1} \text{kpc}^{-2}$ ),  $12 + \log(\text{O}/\text{H})$  and the axial ratio  $b/a$ , respectively. In each panel, the sample is binned in corresponding parameters, and the median values with  $1\sigma$  dispersions in each bin are shown. The grey dashed line represents  $\Delta E(B - V) = 0$ .

limited. If we adopt  $\gamma$  to be  $-0.4$  for all metallicities, the distribution of  $\Delta E(B - V)$  slightly changes.

We do similar analysis on how  $E(B - V)$  varies as a function of  $H\alpha$  surface brightness and inclination in the metallicity bins, because the  $H\alpha$ (SFR) surface density is believed to physically link with the gas surface density, which is closely coupled with dust. Besides, the gas surface density is provided by the current models of galaxy formation. Therefore,  $E(B - V)$  as a function of  $H\alpha$  surface brightness will enable direct application of the empirical relation on the intrinsic reddening in the galaxy evolution models.

Fig. 7 shows  $B_{H\alpha}$  versus  $E(B - V)$  and the best-fitting curve of a power-law function for the face-on objects in the left-hand column, while the distribution of the  $E(B - V)$  ratio against the axial ratio for the three selected metallicity bins in the right-hand column. In each metallicity bin, we fit the data with a function in the form of

$$E(B - V) = p B_{H\alpha, 40}^q (b/a)^\gamma, \quad (11)$$

where  $B_{H\alpha, 40} \equiv B_{H\alpha}/(10^{40} \text{ erg s}^{-1} \text{kpc}^{-2})$ . All the fitting parameters are listed in Table 3. We also fit  $p$  with an exponential function of

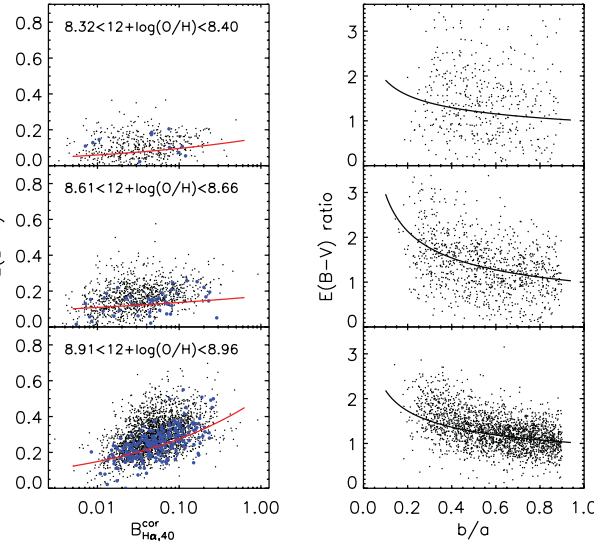


**Figure 7.** Left-hand column:  $\log B_{\text{H}\alpha}$  versus  $E(B - V)$ .  $B_{\text{H}\alpha}$  is in units of  $\text{erg s}^{-1} \text{kpc}^{-2}$ . Right-hand column: the  $E(B - V)$  ratio versus the axial ratio  $b/a$  for each metallicity bin. The  $E(B - V)$  ratio is the ratio of  $E(B - V)$  in other galaxies to that deduced from the best-fitting power law of  $B_{\text{H}\alpha}$  for face-on galaxies. The three metallicity bins are  $0.5, 1$  and  $2 Z_{\odot}$ , as marked in the left-hand column. The symbols and the lines are the same as in Fig. 4.

$12 + \log(\text{O/H})$ , with  $q$  constant, and  $\gamma$  as a step function (Fig. 5):

$$\begin{aligned} p &= (0.092 \pm 0.001) \exp\left(\frac{x}{0.61 \pm 0.01}\right) \\ &= (0.27 \pm 0.02) \left(\frac{Z}{Z_{\odot}}\right)^{0.71 \pm 0.01}, \end{aligned} \quad (12)$$

$$\langle q \rangle = 0.23 \quad (13)$$

and

$$\begin{aligned} \gamma &= -0.2 && \text{for } 0.1 < x < 0.5 \\ &= -0.4 && \text{for } 0.5 \leq x < 1.2. \end{aligned} \quad (14)$$

**Table 3.** Coefficients of empirical fits to reddening in a function such as equation (11).<sup>a</sup>

Metallicity bin	Number of galaxies	$p$	$q$	$\gamma$	$\chi^2_v$
$12 + \log(\text{O/H}) < 8.22$	423	$0.131 \pm 0.003$	$0.286 \pm 0.009$	$-0.298 \pm 0.020$	9.85
$8.22 < 12 + \log(\text{O/H}) < 8.32$	448	$0.147 \pm 0.006$	$0.215 \pm 0.013$	$-0.154 \pm 0.027$	8.78
$8.32 < 12 + \log(\text{O/H}) < 8.40$	515	$0.163 \pm 0.005$	$0.226 \pm 0.011$	$-0.281 \pm 0.027$	7.24
$8.40 < 12 + \log(\text{O/H}) < 8.46$	539	$0.223 \pm 0.006$	$0.263 \pm 0.010$	$-0.149 \pm 0.022$	6.54
$8.46 < 12 + \log(\text{O/H}) < 8.51$	568	$0.205 \pm 0.005$	$0.229 \pm 0.008$	$-0.309 \pm 0.020$	5.34
$8.51 < 12 + \log(\text{O/H}) < 8.56$	733	$0.242 \pm 0.006$	$0.275 \pm 0.008$	$-0.411 \pm 0.018$	5.97
$8.56 < 12 + \log(\text{O/H}) < 8.61$	819	$0.243 \pm 0.004$	$0.249 \pm 0.006$	$-0.400 \pm 0.015$	6.91
$8.61 < 12 + \log(\text{O/H}) < 8.66$	1088	$0.236 \pm 0.004$	$0.221 \pm 0.005$	$-0.472 \pm 0.012$	5.89
$8.66 < 12 + \log(\text{O/H}) < 8.71$	1329	$0.285 \pm 0.004$	$0.229 \pm 0.004$	$-0.391 \pm 0.010$	6.31
$8.71 < 12 + \log(\text{O/H}) < 8.76$	1583	$0.295 \pm 0.004$	$0.236 \pm 0.004$	$-0.488 \pm 0.010$	5.93
$8.76 < 12 + \log(\text{O/H}) < 8.81$	1917	$0.325 \pm 0.003$	$0.229 \pm 0.003$	$-0.457 \pm 0.008$	6.43
$8.81 < 12 + \log(\text{O/H}) < 8.86$	2162	$0.363 \pm 0.003$	$0.227 \pm 0.003$	$-0.415 \pm 0.007$	6.58
$8.86 < 12 + \log(\text{O/H}) < 8.91$	2456	$0.355 \pm 0.003$	$0.189 \pm 0.003$	$-0.406 \pm 0.006$	6.77
$8.91 < 12 + \log(\text{O/H}) < 8.96$	2551	$0.413 \pm 0.003$	$0.194 \pm 0.002$	$-0.339 \pm 0.005$	8.24
$8.96 < 12 + \log(\text{O/H}) < 9.01$	2191	$0.479 \pm 0.003$	$0.227 \pm 0.003$	$-0.347 \pm 0.005$	8.42
$9.01 < 12 + \log(\text{O/H}) < 9.06$	1652	$0.530 \pm 0.003$	$0.248 \pm 0.003$	$-0.346 \pm 0.006$	9.26
$9.06 < 12 + \log(\text{O/H}) < 9.11$	1052	$0.567 \pm 0.004$	$0.286 \pm 0.003$	$-0.410 \pm 0.007$	10.98
$12 + \log(\text{O/H}) > 9.11$	590	$0.526 \pm 0.005$	$0.244 \pm 0.004$	$-0.399 \pm 0.009$	11.22

<sup>a</sup>Empirical relation of  $E(B - V)$  as a function of  $B_{\text{H}\alpha}$  and axial ratio  $b/a$  in different metallicity bins.

with the minimum of scatter (0.28 mag) in the extinction residual  $\Delta A_{\text{H}\alpha} \equiv A_{\text{H}\alpha}^{\text{obs}} - A_{\text{H}\alpha}^{\text{model}}$ , less than the scatter for the SFR model and metallicity model, both of which are 0.33 mag. When calculating  $A_{\text{H}\alpha}$ , they adopt the Calzetti et al. (2000) dust attenuation curve. We repeat their analysis for our selected sample of disc galaxies and compare the scatter of  $\Delta A_{\text{H}\alpha}$  among different models. In each model, a low-order (third-order) polynomial is adopted to fit the extinction, and the distribution of  $\Delta A_{\text{H}\alpha}$  is well fitted by a Gaussian, with widths  $\sigma = 0.27, 0.28$  and  $0.28$  mag for the  $M_*, L_{\text{H}\alpha}$ (SFR) and metallicity models, respectively. Higher order polynomial fits will not decrease the scatter. We check the scatter of  $\Delta A_{\text{H}\alpha}$  for our  $(L_{\text{H}\alpha}, Z, b/a)$  or  $(B_{\text{H}\alpha}, Z, b/a)$  model assuming Calzetti's attenuation law, and the Gaussian width is only  $\sigma = 0.22$  mag [corresponding to  $\sigma = 0.065$  mag for the  $\Delta E(B - V)$  distribution]. We also check for the  $(M_*, Z, b/a)$  model, and find that the scatter of  $\Delta A_{\text{H}\alpha}$  is 0.24 mag, which is better than the single-parameter models, but worse than the other two multiparameter models.

Our empirical relations predict dust reddening better than the single-parameter models, probably because we include disc inclination in the analysis. In order to investigate what dominates the relationships of the variables, we apply principal component analysis on the physical variables. The derived principal components (PCs) are linear combinations of the variables, and represent for the directions of maximum variance in the data. For  $\text{H}\alpha$  luminosity and surface brightness,  $E(B - V)$ ,  $M_*$  and metallicity, the quantities are normalized to zero mean and standard deviation of unity, while for the axial ratio the original value is used. We test with different subsets of variables adopted in each multiparameter model as well as all of the variables, and find similar results. Considering the case of the  $(L_{\text{H}\alpha}, Z, b/a)$  model, for example, the first two PCs contribute to about 80 per cent of the total variance. In PC1, the variables  $L_{\text{H}\alpha}$ ,  $Z$  and  $E(B - V)$  weight almost equivalently. This is consistent with what Garn & Best (2010) found. However, in PC2 the axial ratio weights the most ( $-0.98$ ) and  $E(B - V)$  weights the second ( $0.30$ ). The result is consistent with what we previously found. Although the axial ratio only weakly correlated with  $E(B - V)$  ( $r_s = -0.13$ ,  $P_{\text{null}} < 10^{-5}$ ), after removing the  $E(B - V)$  dependence on  $\text{H}\alpha$  luminosity and metallicity, the negative correlation between  $b/a$  and  $E(B - V)$  emerges.

## 4.2 Error analysis

We have shown that the global reddening of the emission lines from a disc galaxy can be reasonably determined by its  $\text{H}\alpha$  luminosity or surface brightness, gas metallicity and disc inclination. The  $1\sigma$  scatter of  $\Delta E(B - V)$  is about 0.07 mag, which is contributed by several sources, including the measurement uncertainty in the Balmer decrement, the error in the metallicity, the uncertainties in other variables and the intrinsic scatter in the relation. We will discuss the uncertainties in the following.

Let us take a review of the uncertainties in the physical quantities. The formal error for  $L_{\text{H}\alpha}$  measurement is 0.04 dex, and for  $B_{\text{H}\alpha}$  is 0.05 dex. As discussed in Section 3.2, the uncertainty induced by aperture correction and attenuation correction is less than 0.12 dex. The typical error of  $b/a$  is 0.02. The uncertainty in metallicity calibration dominates the uncertainty of metallicity, estimated to be  $\sim 0.15$  dex. We use Monte Carlo simulation to estimate the error of  $E(B - V)$  for equations (7) and (11) taking the uncertainties for the best-fitting parameters and the measurement errors for the physical variables. The errors of  $E(B - V)$  predicted by equations (7) and (11) are both about 0.056 mag. If we take the uncertainty in aperture correction and attenuation correction (0.12 dex at most) into account

in  $L_{\text{H}\alpha}$  and  $B_{\text{H}\alpha}$  error, then the simulated  $E(B - V)$  errors slightly change to 0.058 mag. Remember that the measurement error of  $E(B - V)$  is 0.03 mag, and the scatter of  $\Delta E(B - V)$  (0.07 mag) can be almost explained by the uncertainties of the physical quantities. Considering all these uncertainties, the  $E(B - V)$  values predicted from the empirical relations are quite consistent with the observed values.

From Fig. 6 we can see that the  $\Delta E(B - V)$  distribution can be well described by a Gaussian profile, indicative of a random distribution. However, the intrinsic scatter of the empirical relation is still unclear, because of the large uncertainty in the metallicity calibration. Therefore, to estimate the intrinsic scatter of the relation, it will be of help to decrease the uncertainty in the metallicity calibration and obtain the metallicity more precisely. One may find there is slight excess over the positive tail of the Gaussian distribution. We examine the objects (about 1 per cent of the whole sample) with  $\Delta E(B - V) > 0.2$ , that is, the observed  $E(B - V)$  is underestimated with our empirical models by 0.2 mag, and find that these objects are prone to large Balmer decrement, low  $\text{H}\beta$  S/N and low  $\text{H}\beta$  EW.

As previously mentioned, we require  $S/N > 20$  for  $\text{H}\alpha$ , and  $S/N > 10$  for  $\text{H}\beta$  and  $[\text{O}\text{III}]$  when selecting our sample in Section 2. The  $S/N$  criteria for  $\text{H}\alpha$  will exclude some galaxies with low SFR and low  $\text{H}\alpha$  EW. Thus, the number of galaxies with low  $\text{H}\alpha$  luminosity and low SFR will be reduced. In fact, when the criterion  $S/N > 10$  is applied for  $\text{H}\beta$ , most of the remaining sample ( $\sim 99.9$  per cent) will have  $\text{H}\alpha$   $S/N > 20$ . In order to investigate whether the  $\text{H}\beta$  and  $[\text{O}\text{III}]$   $S/N$  criteria bias our results, we attempt a looser  $S/N (> 5)$  criterion for both lines, and the sample is expanded by 50 per cent to have 34 815 galaxies. Then we fit the data with both the  $(L_{\text{H}\alpha}, Z, b/a)$  model and the  $(B_{\text{H}\alpha}, Z, b/a)$  model. The results show that the fit parameters are quite similar to those we have obtained earlier in this section, but the scatter in  $\Delta E(B - V)$  increases to about 0.08 mag. Note that 10 per cent uncertainty in  $\text{H}\alpha/\text{H}\beta$  will result in an uncertainty of 0.086 mag in  $E(B - V)$ , which explains the increased scatter. Thus, including the low- $S/N$  objects merely introduces more scatter in the relation.

## 5 A TOY MODEL ON DUST EXTINCTION TO H II REGIONS IN A DISC GALAXY

Two different sources contribute to the extinction for H II regions: dust associated with the individual H II regions and diffuse foreground dust in the galaxy. Let us first consider the dust in the precursor molecular clouds (MCs). The intrinsic extinction in individual H II regions depends on the relative distribution of young massive stars, gas and dust in the star formation regions, which are also closely related to the age and size of the precursor MCs, as well as the stochastic formation of high-mass stars for a given IMF. An H II region is embedded in a cold gas/dust envelope before the cold gas/dust is blown away. The time-scale for such a process is expected to depend on the size and density of the precursor cloud: longer for more massive and dense H II regions. Panuzzo et al. (2003) discussed the attenuation to the  $\text{H}\alpha$  emission line for different evaporating time-scales, in comparison with the lifetime of massive stars that produce the ionizing continuum. They simply adopt a central ionizing star in a spherical cloud, which corresponds to the maximum attenuation case. If the time-scale is short enough, most H II regions are produced outside the MC, and the main attenuation is due to foreground dust. In the case of long evaporation time, an H II region is buried in the MC during most of their lifetime and the extinction associated with the H II region will be important. In a galaxy, all these cases are likely present. Furthermore, the young

ionizing stars are not necessarily forming in the cloud centre. These complications make any prediction of the reddening in an individual cloud rather difficult.

However, as far as a large number of H II regions are concerned, the statistical behaviour may be quite well defined. The H $\alpha$  luminosity function of H II regions in spiral galaxies can be described by double-power-law functions, with a flatter power law below the break luminosity of 38.6 (in units of erg s $^{-1}$ , logarithmic), and a steeper one above it (e.g. Kennicutt, Edgar & Hodge 1989; Bradley et al. 2006). In our sample, most galaxies have H $\alpha$  luminosities above 40 (in units of erg s $^{-1}$ , logarithmic) with a median of 41.5, and the maximum is 43.3. Therefore, a galaxy consists of numerous (of the order of hundreds to millions of) H II regions. The H II regions follow certain distributions of ages and initial masses, determined by the star formation processes, because the star formation time in a galaxy is likely much longer than the lifetime of an individual H II region, that is, the lifetime of OB stars. If these distributions are the same for each galaxy and there are a large number of H II regions, one may expect that the average extinction within H II regions should be similar in each galaxy. In this respect, it is not expected that the dust reddening depends on the H $\alpha$  luminosity or the inclination of the disc. In contrast, for example, if the MC mass function and stellar IMF depend on the global properties of the galaxies, such as the gas surface density, then one may expect that the average extinction is correlated with the global properties. However, this is poorly known so far.

Next, we consider the extinction due to diffuse interstellar dust in a galaxy. It is expected that this extinction depends on the gas surface density, inclination, metallicity of the interstellar medium and size of the galaxy. To simplify the model, we will adopt smooth distributions for the dust, gas and star formation regions with the following assumptions:

(1) Dust-to-gas density ratio is proportional to gas metallicity (Issa, MacLaren & Wolfendale 1990), that is, gas and dust are coupled:

$$\rho_d \propto \rho_g \times Z, \quad (15)$$

where  $\rho_d$  and  $\rho_g$  are the dust density and gas density, respectively.

(2) Both gas and dust distributions in the vertical ( $z$ ) and radial ( $R$ ) directions can be described by an exponential law (e.g. de Jong 1996; Thomas et al. 2004; Misiriotis et al. 2006), that is,

$$\rho_g = \rho_{g0} \exp(-z/h_g) \exp(-R/R_g), \quad (16)$$

where  $\rho_{g0}$  is the gas density at  $z = 0$  and  $R = 0$ , and  $h_g$  and  $R_g$  are the characteristic lengths in the vertical and radial directions, respectively, for gas distribution. However, the dust distribution may have different length-scales due to radial metallicity gradient:

$$\rho_d = \rho_{d0} \exp(-z/h_d) \exp(-R/R_d), \quad (17)$$

where  $\rho_{d0}$  is the dust density at  $z = 0$  and  $R = 0$ , and  $h_d$  and  $R_d$  are the characteristic lengths in the vertical and radial directions, respectively, for dust distribution.

(3) The H II distribution is also exponential in both the radial and the vertical direction, but with different characteristic lengths (e.g. de Jong 1996):

$$\rho_{H\alpha} = \rho_{H\alpha0} \exp(-z/h_{H\alpha}) \exp(-R/R_{H\alpha}). \quad (18)$$

By integrating  $\rho_{H\alpha}$  over the  $z$  direction, we yield a surface density of H $\alpha$ ,  $\Sigma_{H\alpha}$ . Specifically, the H $\alpha$  surface density at  $R = 0$  is

$$\begin{aligned} \Sigma_{H\alpha,0} &= \int_0^\infty \rho_{H\alpha}(0) \exp(-z/h_{H\alpha}) dz + \int_{-\infty}^0 \rho_{H\alpha}(0) \exp(z/h_{H\alpha}) dz \\ &= 2\rho_{H\alpha}(0)h_{H\alpha}. \end{aligned} \quad (19)$$

The gas disc is rather thin in general. As a result, dust attenuation can be modelled as plane parallel except at extremely high inclinations. Young stars are formed in dense molecular cores, which might be distributed in a plane thinner than the gas disc. For a plane-parallel model, the optical depth is expressed as

$$\tau = \rho_d k_v z / \cos i, \quad (20)$$

where  $k_v$  is the opacity coefficient and  $i$  is the inclination angle, and  $i = 0^\circ$  represents the line of sight perpendicular to the galaxy disc, while  $i = 90^\circ$  represents the line of sight parallel to the galaxy disc. The optical depth to H $\alpha$  emission from the middle plane of the disc to the upper disc surface at  $R = 0$  is defined as

$$\tau_{H\alpha,0} = \int_0^\infty \rho_d(0) k_v \exp(-h/h_d) dh = \rho_d(0) k_v h_d. \quad (21)$$

It is symmetric between the middle plane and the upper and lower disc surfaces; thus, the overall optical depth through the whole disc vertically at  $R = 0$  should be  $2\tau_{H\alpha,0}$ . Then, the optical depth from the point at  $z(>0)$  on the vertical axis ( $R = 0$ ) to the upper surface of the disc is

$$\tau_1(z) = \int_z^\infty \rho_d(0) k_v \exp(-h/h_d) dh = \tau_{H\alpha,0} \exp(-z/h_d), \quad (22)$$

and the optical depth from that point to the lower disc surface can be expressed as

$$\tau_2(z) = 2\tau_{H\alpha,0} - \tau_1(z). \quad (23)$$

Light from the H II regions at the position ( $z, R$ ) needs to travel through the disc, from both the upper and the lower sides. With these descriptions, we can calculate the H $\alpha$  luminosity, H $\alpha$  surface brightness and average attenuation at H $\alpha$  and H $\beta$  by integrating the radiation transfer function over both the vertical and the radial direction within the disc. Then the H $\alpha$  luminosity is

$$L_{H\alpha} = \int_0^2 \pi d\theta \int_0^{R_{H\alpha,\max}} RdR \int_0^\infty \rho_{H\alpha} \left\{ \exp \left[ -\frac{\tau_1(z)}{\cos i} \exp(-R/R_d) \right] + \exp \left[ -\frac{\tau_2(z)}{\cos i} \exp(-R/R_d) \right] \right\}. \quad (24)$$

Substituting equations (18), (22), (23),  $y = \exp(-z/h_{H\alpha})$  and  $a = R/R_{H\alpha}$  into equation (24), we get

$$\begin{aligned} L_{H\alpha} &= \pi R_{H\alpha}^2 \Sigma_{H\alpha,0} \int_0^1 dy \int_0^\xi da \exp(-a) \\ &\quad \left\{ \exp \left[ -\frac{\tau_{H\alpha,0}}{\cos i} \exp(-a/\eta) y^{1/\kappa} \right] \right. \\ &\quad \left. + \exp \left[ -\frac{\tau_{H\alpha,0}}{\cos i} \exp(-a/\eta) (2 - y^{1/\kappa}) \right] \right\}, \end{aligned} \quad (25)$$

where  $\xi \equiv R_{H\alpha,\max}/R_{H\alpha}$  is set by the threshold surface density of star formation  $R_{H\alpha,\max} \equiv R_g \ln(\Sigma_{g,0}/\Sigma_{th})$ , and the threshold gas surface density is adopted as  $\Sigma_{th} \simeq 5 M_\odot \text{ pc}^{-2}$  (Martin & Kennicutt 2001);  $\Sigma_{g,0}$  is the surface density of gas at  $R = 0$ ;  $\eta = R_d/R_{H\alpha}$ ; and  $\kappa = h_d/h_{H\alpha}$ . In order to reduce the number of free parameters ( $\Sigma_{H\alpha,0}$ ,  $\tau_{H\alpha,0}$ ,  $\cos i$ ,  $\xi$ ,  $\eta$  and  $\kappa$ ), we use the empirical relation between SFR surface density,  $\Sigma_{SFR}$ , and gas surface density  $\Sigma_g$  (known as the Kennicutt–Schmidt law; Kennicutt et al. 1998):

$$\begin{aligned} \Sigma_{SFR} (\text{M}_\odot \text{ yr}^{-1} \text{ kpc}^{-2}) \\ = (2.5 \pm 0.7) \times 10^{-4} \left( \frac{\Sigma_g}{\text{M}_\odot \text{ pc}^{-2}} \right)^{1.4 \pm 0.15}. \end{aligned} \quad (26)$$

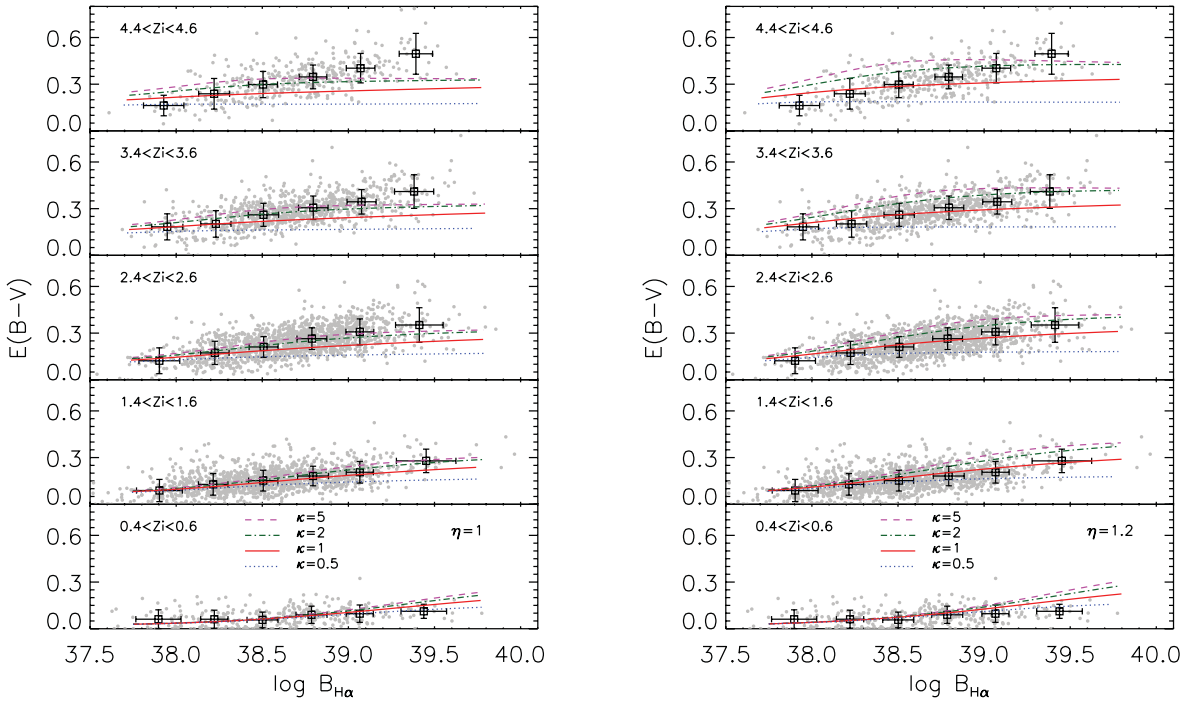


**Figure 8.** Average surface brightness  $B_{H\alpha}$  ( $\text{erg s}^{-1} \text{kpc}^{-2}$ , corrected for extinction) versus  $E(B-V)$ , with the relative characteristic lengths of dust distribution to H II regions in the radial direction,  $\eta = 1$  (left-hand column) and  $\eta = 1.2$  (right-hand column). Observation samples with  $Z/\cos i$ , marked as  $Zi$  for short, in bins of  $0.5 \pm 0.1$ ,  $1.5 \pm 0.1$ ,  $2.5 \pm 0.1$ ,  $3.5 \pm 0.1$  and  $4.5 \pm 0.1$  are shown. The dotted (blue) line represents the relative characteristic lengths of dust distribution to H II regions in the vertical direction,  $\kappa = 0.5$ , solid (red) line for  $\kappa = 1$ , dashed (magenta) line for  $\kappa = 2$ , and dot-dashed (green) line for  $\kappa = 5$ .

Considering that the gas and H II distributions are both exponential, we get  $R_g = 1.4R_{H\alpha}$ . With above relations and the conversion between  $L_{H\alpha}$  and SFR (equation 3), we can write

$$\xi = \ln \frac{\Sigma_{H\alpha,0}}{4.4 \times 10^{38} \text{ erg s}^{-1} \text{kpc}^{-2}}. \quad (27)$$

Assuming the dust-to-gas ratio to be the same as in the Galactic disc, that is,  $E(B-V) = 1.7 \times 10^{-22} N_{\text{H}}(Z/Z_{\odot})$  (Bohlin, Savage & Drake 1978), and a Galactic extinction curve (Fitzpatrick 1999), we obtain the effective optical depth to  $H\alpha$  through the disc perpendicularly as

$$\tau_{H\alpha,0} = 0.5 \left( \frac{\Sigma_{H\alpha,0}}{3.3 \times 10^{39} \text{ erg s}^{-1} \text{kpc}^{-2}} \right)^{0.714} \frac{Z}{Z_{\odot}}. \quad (28)$$

Once we have  $\tau$ , it is straightforward to calculate the extinction at  $H\alpha$  using equation (25) as given below:

$$\begin{aligned} A_{H\alpha} &= -2.5 \log \left( \frac{L_{H\alpha,\tau}}{L_{H\alpha,\tau=0}} \right) \\ &= \int_0^1 dy \int_0^\xi da d\alpha \exp(-a) \left\{ \exp \left[ -\frac{\tau_{H\alpha,0}}{\cos i} \exp(-a/\eta) y^{1/\kappa} \right] \right. \\ &\quad \left. + \exp \left[ -\frac{\tau_{H\alpha,0}}{\cos i} \exp(-a/\eta) (2 - y^{1/\kappa}) \right] \right\} / \\ &\quad 2[1 - \exp(-\xi) - \xi \exp(-\xi)]. \end{aligned} \quad (29)$$

Similarly, replacing  $\tau_{H\alpha,0}$  with  $\tau_{H\beta,0}$ , one obtains the extinction at  $H\beta$ . Thus, the  $H\alpha/H\beta$  ratio can be calculated, and then  $L_{H\alpha}$  can be corrected with the extinction estimated from the Balmer decrement, as the extinction correction we make to the observed  $L_{H\alpha}$ .

In order to examine if such a model can reproduce the observed correlations, we compute the average surface brightness  $B_{H\alpha}$  and

colour excess  $E(B-V)$  estimated by  $H\alpha/H\beta$  from the model based on the following parameters:  $\Sigma_{H\alpha,0}$ ,  $Z$ ,  $\cos i$ ,  $\eta$  and  $\kappa$ . To facilitate comparison with observations, we obtain  $B_{H\alpha}$  following the same method as used for observations (equation 6) by dividing the attenuation-corrected  $L_{H\alpha}$  with the surface within the half-light radius, defined as the radius within which the  $H\alpha$  luminosity is half of the total  $L_{H\alpha}$ . The  $E(B-V)$  is calculated from  $A_{H\alpha}$  and  $A_{H\beta}$  assuming Fitzpatrick's extinction curve. We first fix  $\eta$  to be 1. Since increasing metallicity and inclination both cause an increase in extinction, these two factors are coupled in the model. Therefore, we incorporate them into one parameter  $Zi \equiv Z/\cos i$ . We compute the models for a grid of parameters with  $38.5 < \log \Sigma_{H\alpha,0} < 42.0$ ,  $Zi = 0.5, 1.5, 2.5, 3.5, 4.5$ ,  $\kappa = 0.5, 1, 2, 5$ .

The models are overplotted on the observation sample in the  $B_{H\alpha}$  versus  $E(B-V)$  plane (Fig. 8). For clarity, we only show the observation sample in five bins of  $Zi$  with a bin width of 0.2, and on each panel the subsample is binned in  $B_{H\alpha}$  and shown in squares with error bars. We can see the observation trend in each panel that  $E(B-V)$  increases as  $B_{H\alpha}$  increases. The model curves are calculated with the corresponding value of median  $Zi$  for each subsample. In each panel,  $E(B-V)$  gets larger when  $\kappa$  increases, and each curve with constant  $\kappa$  first increases and then becomes flat as  $B_{H\alpha}$  increases. At small  $\kappa$ , that is, the dust layer is much thinner than the stellar disc,  $E(B-V)$  saturates at a small value because the Balmer line emission from the disc of larger height tends to dominate, resulting in a small  $E(B-V)$ , while at large  $\kappa$  more Balmer line emission comes from the inner region close to the mid-plane of the disc, thus tends to have a large  $E(B-V)$ . The saturation is due to the fact that the observed light from outside weights more as the optical depth increases.

Generally, the  $\kappa = 1$  model reproduces the observed correlations at low  $Zi$ . However, as  $Zi$  increases, the constant- $\kappa$  model is lower

than the observation trend at the high end of  $B_{\text{H}\alpha}$ . At medium  $Zi$  ( $1.5 \sim 2.5$ ), the observation can be better presented by the model with larger  $\kappa$  (e.g.  $\kappa \geq 2$ ). This could be explained by the vertical expansion of dust distribution in the disc, while higher surface brightness indicates more intense star formation activity. The dust may be driven away from the mid-plane of the disc by radiation pressure or the stellar winds; thus, the dust layer becomes thicker than that for low  $B_{\text{H}\alpha}$ . However,  $E(B - V)$  saturates at about 0.3 mag when  $\kappa \geq 2$ , which means that the effective optical depth saturates when the height of dust layer gets to twice the height of H II regions. Another possible explanation is that the Kennicutt–Schmidt law we adopt in the model is an averaged star formation law that links between the surface density of gas and star formation in the form of  $\Sigma_{\text{SFR}} \propto \Sigma_g^N$ . Leroy et al. (2008) suggested that the star formation law may vary as a function of local conditions at different galactocentric radii, including metallicity and the dominated gas content (H I or H<sub>2</sub>). The star formation law has smaller  $N$  value at higher  $\Sigma_{\text{SFR}}$  in the inner region of a galaxy (e.g. Bigiel et al. 2008, their fig. 11); thus, large dust reddening in the inner region dominates the observed  $E(B - V)$ . As a result, the dust reddening is higher than predicted by the present model.

In the model above, we assume  $\eta = 1$ , that is, the dust and H II region have the same characteristic scale in the radial distribution, but the gas/dust may distribute at larger radii than the star-forming regions (e.g. Bigiel et al. 2008). Thus, we also consider  $\eta = 1.2$ , and find that the observation with large  $Zi$  can be well explained by a model with  $\kappa = 1$  at low  $B_{\text{H}\alpha}$  and  $\kappa \geq 2$  at high  $B_{\text{H}\alpha}$ . It is possible because in a spiral galaxy centre, where the metallicity is higher than outside, we are observing the star formation dominated centre, and the gas (or dust) distribution is more extended.

In this simple toy model, the optical depth  $\tau_{\text{H}\alpha}$  is assumed to be proportional to the metallicity  $Z$ . It comes from the assumption that  $\rho_d \propto \rho_g \times Z$ . However, there is evidence that this assumption may not be the case in practice. Boissier et al. (2004) studied six nearby late-type galaxies in far-IR and UV images, and find that the dust-to-gas density ratio is proportional to  $(Z/Z_\odot)^{0.88}$ , which was flatter than the linear correlation we adopted above. This suggests that the dust-to-gas density ratio may not evolve linearly with  $Z$ . In addition, we assume in the model that the disc height is very thin, that is, the disc height is quite small compared to the disc radius; thus, the radial gradient in gas density can be neglected when calculating  $\tau_{\text{H}\alpha}$ . Under that assumption, the effect of inclination on optical depth can be expressed as  $(\cos i)^{-1}$ . However, the disc height may not be the same at all radii in practice. For instance, the disc may be thicker in the centre than in the outer region or the bulge is present in the disc centre. Also, the distribution of dust and star formation regions may not be smooth, for example, when the spiral arms are present in the disc galaxy. In those cases, the inclination factor might be flatter than  $(\cos i)^{-1}$ . Accounting for these realistic effects, we adjust  $Z/Z_\odot$  to  $(Z/Z_\odot)^\alpha$  in equation (28) and  $(\cos i)^{-1}$  to  $(\cos i)^{-\alpha}$  in equations (25) and (29), then test several values for the power-law index.<sup>6</sup> It turns out that with  $\alpha = 0.7$  the simple model reproduces the observation trend well (Fig. 9). When  $Zi$  is low, the model of constant  $\kappa$  (0.5 or 1) reproduces the observation trend well. While  $Zi$  is higher, the observation can be reproduced with the model of  $\kappa \geq 2$ .

<sup>6</sup> Because the metallicity and inclination are coupled in this simply toy model, the power-law index of  $\cos i$  is adopted to be the same as that of  $Z$ , so as to be incorporated into  $Zi$ .

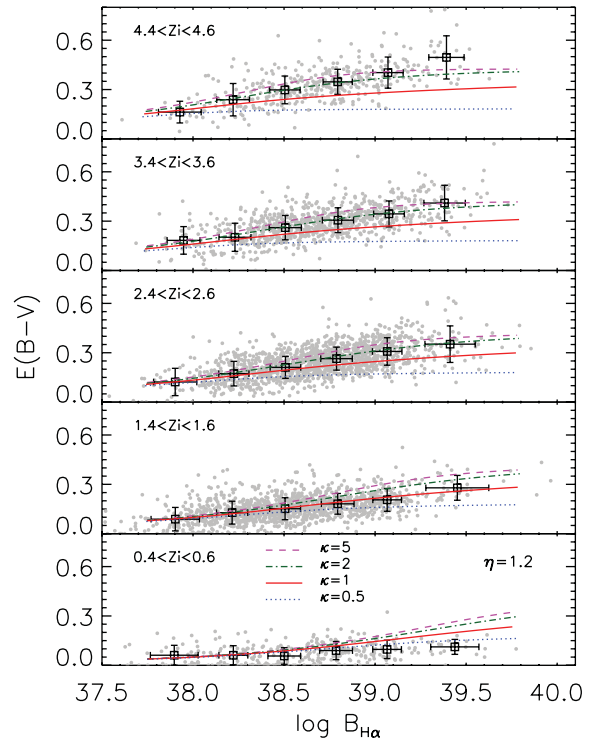


Figure 9. Same as Fig. 8, except that the model is calculated with equations (28) and (29), but after adjusting  $Z/Z_\odot$  to  $(Z/Z_\odot)^{0.7}$  and  $\cos i$  to  $(\cos i)^{0.7}$ .

To summarize, the simple toy models reproduce the observed trend between dust reddening and H $\alpha$  surface brightness, that is, reddening increases with increase in  $B_{\text{H}\alpha}$ . The comparisons between observations and the toy models indicate that the relative distribution of H II regions to gas/dust both in the vertical and in the radial directions of the galaxy disc may vary in different environments of star formation activity levels or metallicities. The dust might be distributed farther beyond the H II regions when the star formation activity is more intense, or the dust is distributed in a thicker disc ( $\kappa \geq 1$ ) than the H II regions when the metallicity gets higher. In addition, our results imply that the dust-to-gas density ratio may not be proportional to metallicity  $Z$ , but to a power law of  $Z$ ,  $Z^\alpha$  with  $\alpha \sim 0.7$ .

## 6 CONCLUSIONS AND IMPLICATIONS

We present the empirical formulae of intrinsic reddening as a function of intrinsic H $\alpha$  luminosity or surface brightness, metallicity and disc inclination (equations 7 and 11 and Tables 2 and 3) for a large sample of  $\sim 22\,000$  well-defined star-forming disc galaxies selected from SDSS DR5. With the empirical formulae, the reddening parametrized by  $E(B - V)$  could be predicted within  $1\sigma$  uncertainty of 0.07 mag.  $\Delta E(B - V)$ , defined as the observed reddening estimated from the Balmer decrement minus predicted value, does not correlate with the three parameters used in the formulae. We also find that  $\Delta E(B - V)$  is independent of the stellar mass, 4000 Å break strength or electron density within the galaxy.

The observed trend between dust reddening and H $\alpha$  surface brightness could be reproduced by a plane-parallel slab toy model, in which the dust is scaled with gas, and all the distributions of the dust, gas and star formation regions are smooth and follow exponential laws in the disc. We find from the comparisons of the models with the observation that the relative vertical scale of dust

distribution to H II regions may vary with H $\alpha$  surface brightness or metallicity. The higher intensity of star formation could drive the dust to distribute in a thicker layer, or the dust disc is thicker than the disc of the H II regions when the metallicity is higher. However, the real galaxies may not be fully described by this simple toy model. For example, when the spiral arms are present, or the star formation regions are clumpy, the assumptions of smooth distributions will be improper. In addition, our result implies a different scaling law of dust-to-gas density ratio as a function of metallicity  $Z$  from the linear relation (equation 15). Our empirical relations, which suggest dust reddening is partially dependent on metallicity ( $\propto Z^{0.6 \sim 0.7}$ ), can be an observational constraint on the output of radiative transfer model calculations, and hence provides constraints on the assumed dust-to-gas density ratio in the model.

Since metallicity dependence has been introduced, we believe that our empirical formulae should be applicable to the early evolutionary stage of a galaxy, when the gas metallicity might be low. In the starburst galaxies at high redshift, dust surrounding star-forming regions has been proven to be prone to submillimetre and far-IR observations. However, most of those galaxies are relatively dim in the optical, implying severe extinction and reddening to these galaxies. The observed galaxies at high redshifts are affected by reddening, to the extent that the galaxies with heavy attenuation and reddening may escape detection. The importance of the reddening correction depends on the wavelength band that is used. For example, UV continuum luminosity is usually used to infer SFR in high-redshift galaxies. It is very sensitive to attenuation/reddening. Calzetti et al. (2000) find that the extinction to emission lines and extinction to stellar continua in the optical band are different, and the continuum reddening is only about 40 per cent of that for emission lines. However, the extinction to UV continua is likely similar to H II regions because UV continua are also emitted by young hot stars, which are likely surrounded by H II regions. As a result, our results may be used to estimate the reddening for these high-redshift galaxies with caution that the metallicity should be well calibrated and be within the range covered by our sample. Following equation (7) and the discussions in Section 4, the SFR in luminous star formation or high-metallicity galaxies might have been underestimated (e.g. Heckman et al. 1998; Hopkins et al. 2001; Panuzzo et al. 2007), or those galaxies are even completely lost in optical surveys.

The quantitative relationship of reddening with metallicity, luminosity or surface brightness, and the inclination for disc galaxies can also be incorporated into the current semi-analytic models of galaxy formation and evolution (e.g. De Lucia et al. 2004; Kang et al. 2005; Croton et al. 2006). In those models, a simple chemical enrichment scheme has been included, and the metal abundance has been actually predicted. With the known metallicity and the SFR (intrinsic luminosity) provided by the models, the reddening can be estimated accurately using our formulae, and then used to shape the SED and predict the emerging luminosity more realistically.

## ACKNOWLEDGMENTS

We would like to thank the anonymous referee for useful suggestions that improved this paper. We thank Gleniese Mckenzie and Peng Jiang for helpful comments on the manuscripts. This work is supported by NSFC (10973013, 11073017, 11033007), 973 Program (2009CB824800) and the Fundamental Research Funds for the Central Universities. Funding for the SDSS and SDSS-II has been provided by the Alfred P. Sloan Foundation, the Participating Institutions, the National Science Foundation, the US Department of Energy, the National Aeronautics and Space Administration,

the Japanese Monbukagakusho, the Max Planck Society, and the Higher Education Funding Council for England. The SDSS website is: <http://www.sdss.org/>. SDSS is managed by the Astrophysical Research Consortium for the Participating Institutions. The Participating Institutions are the American Museum of Natural History, Astrophysical Institute Potsdam, University of Basel, University of Cambridge, Case Western Reserve University, University of Chicago, Drexel University, Fermilab, the Institute for Advanced Study, the Japan Participation Group, The Johns Hopkins University, the Joint Institute for Nuclear Astrophysics, the Kavli Institute for Particle Astrophysics and Cosmology, the Korean Scientist Group, the Chinese Academy of Sciences (LAMOST), Los Alamos National Laboratory, the Max Planck Institute for Astronomy (MPIA), the Max Planck Institute for Astrophysics (MPA), New Mexico State University, Ohio State University, University of Pittsburgh, University of Portsmouth, Princeton University, the United States Naval Observatory, and the University of Washington.

## REFERENCES

- Adelman-McCarthy J. K. et al., 2007, ApJS, 172, 634  
 Afonso J., Hopkins A., Mobasher B., Almeida C., 2003, ApJ, 597, 269  
 Alonso-Herrero A., Rieke G. H., Rieke M. J., Colina L., Pérez-González P. G., Ryder S. D., 2006, ApJ, 650, 835  
 Asari N. V., Cid Fernandes R., Stasińska G., Torres-Papaqui J. P., Mateus A., Sodré L., Schoenell W., Gomes J. M., 2007, MNRAS, 381, 263  
 Asplund M., Grevesse N., Sauval A. J., Allende Prieto C., Kiselman D., 2004, A&A, 417, 751  
 Baldwin J. A., Phillips M. M., Terlevich R., 1981, PASP, 93, 5  
 Balogh M. L., Morris S., Yee H., Carlberg R., Ellingson E., 1999, ApJ, 527, 54  
 Bigiel F., Leroy A., Walter F., Brinks E., de Blok W. J. G., Madore B., Thornley M. D., 2008, AJ, 136, 2846  
 Blanton M. R., Roweis S., 2007, AJ, 133, 734  
 Blanton M. R. et al., 2001, AJ, 121, 2358  
 Bohlin R. C., Savage B. D., Drake J. F., 1978, ApJ, 224, 132  
 Boissier S., Boselli A., Buat V., Donas J., Milliard B., 2004, A&A, 424, 465  
 Bradley T. R., Knapen J. H., Beckman J. E., Folkes S. L., 2006, A&A, 459, L13  
 Brinchmann J., Charlot S., White S. D. M., Tremonti C., Kauffmann G., Heckman T., Brinkmann J., 2004, MNRAS, 351, 1151  
 Bruzual A. G., 1983, ApJ, 273, 105  
 Bruzual A. G., Charlot S., 2003, MNRAS, 344, 1000 (BC03)  
 Buat V., Boselli A., Gavazzi G., Bonfanti C., 2002, A&A, 383, 801  
 Calzetti D., 2001, PASP, 113, 1449  
 Calzetti D., Kinney A. L., Storchi-Bergmann T., 1994, ApJ, 429, 582  
 Calzetti D., Armus L., Bohlin R. C., Kinney A. L., Kormneef J., Storchi-Bergmann T., 2000, ApJ, 533, 682  
 Calzetti D. et al., 2007, ApJ, 666, 870  
 Calzetti D. et al., 2010, ApJ, 714, 1256  
 Chabrier G., 2003, PASP, 115, 763  
 Charlot S., Fall S. M., 2000, ApJ, 539, 718  
 Croton D. J. et al., 2006, MNRAS, 365, 11  
 Dale D. A., Helou G., 2002, ApJ, 576, 159  
 de Jong R. S., 1996, A&A, 313, 377  
 De Lucia G., Blaizot J., 2007, MNRAS, 375, 2  
 De Lucia G., Kauffmann G., White S. D. M., 2004, MNRAS, 349, 1101  
 Denicoló G., Terlevich R., Terlevich E., 2002, MNRAS, 330, 69  
 Dong X.-B., Zhou H.-Y., Wang T.-G., Wang J.-X., Li C., Zhou Y.-Y., 2005, ApJ, 620, 629  
 Dong X.-B. et al., 2007, ApJ, 657, 700  
 Driver S. P., Popescu C. C., Tuffs R. J., Liske J., Graham A. W., Allen P. D., de Propriis R., 2007, MNRAS, 379, 1022  
 Fagotto F., Bressan A., Bertelli G., Chiosi C., 1994a, A&AS, 104, 365  
 Fagotto F., Bressan A., Bertelli G., Chiosi C., 1994b, A&AS, 105, 29  
 Fitzpatrick E. L., 1999, PASP, 111, 63

- Garn T., Best P. N., 2010, MNRAS, 409, 421  
 Garn T. et al., 2010, MNRAS, 402, 2017  
 Garnett D. R., Shields G. A., 1987, ApJ, 317, 82  
 Guiderdoni B., Rocca-Volmerange B., 1987, A&A, 186, 1  
 Heckman T. M., Robert C., Leitherer C., Garnett D. R., van der Rydt F., 1998, ApJ, 503, 646  
 Hopkins A. M., Connolly A. J., Haarsma D. B., Cram L. E., 2001, AJ, 122, 288  
 Iglesias-Páramo J. et al., 2006, ApJS, 164, 38  
 Issa M. R., MacLaren I., Wolfendale A. W., 1990, A&A, 236, 237  
 Kang X., Jing Y. P., Mo H. J., Börner G., 2005, ApJ, 631, 21  
 Kauffmann G., Colberg J. M., Diaferio A., White S. D. M., 1999, MNRAS, 303, 188  
 Kauffmann G. et al., 2003a, MNRAS, 341, 33  
 Kauffmann G. et al., 2003b, MNRAS, 346, 1055 (Ka03)  
 Kennicutt R. C., Jr, 1998, ApJ, 498, 541  
 Kennicutt R. C., Jr, Edgar B. K., Hodge P. W., 1989, ApJ, 337, 761  
 Kewley L. J., Dopita M. A., 2002, ApJS, 142, 35  
 Kewley L. J., Ellison S. L., 2008, ApJ, 681, 1183  
 Kewley L. J., Dopita M. A., Sutherland R. S., Heisler C. A., Trevena J., 2001, ApJ, 556, 121  
 Kewley L. J., Geller M. J., Jansen R. A., 2004, AJ, 127, 2002  
 Kewley L. J., Jansen R. A., Geller M. J., 2005, PASP, 117, 227  
 Kewley L. J., Groves B., Kauffmann G., Heckman T., 2006, MNRAS, 372, 961  
 Kitzbichler M. G., White S. D. M., 2007, MNRAS, 376, 2  
 Kong X., 2004, A&A, 425, 417  
 Kroupa P., 2001, MNRAS, 322, 231  
 Leroy A. K., Walter F., Brinks E., Bigiel F., de Blok W. J. G., Madore B., Thornley M. D., 2008, AJ, 136, 2782  
 Liang Y. C., Yin S. Y., Hammer F., Deng L. C., Flores H., Zhang B., 2006, ApJ, 652, 257  
 Lonsdale C. J. et al., 2003, PASP, 115, 897  
 Lu H., Zhou H., Wang J., Wang T., Dong X., Zhuang Z., Li C., 2006, AJ, 131, 790  
 McGaugh S. S., 1991, ApJ, 380, 140  
 Markwardt C. B., 2009, in Bohlender D. A., Durand D., Dowler P., eds, ASP Conf. Ser. Vol. 411, Astronomical Data Analysis Software and Systems XVIII. Astron. Soc. Pac., San Francisco, p. 251  
 Martin C. L., Kennicutt R. C., Jr, 2001, ApJ, 555, 301  
 Misiriotis A., Xilouris E. M., Papamastorakis J., Boumis P., Goudis C. D., 2006, A&A, 459, 113  
 Nagao T., Maiolino R., Marconi A., 2006, A&A, 459, 85  
 O'Donnell J. E., 1994, ApJ, 422, 158  
 Osterbrock D. E., Ferland G. J., 2006, in Osterbrock D. E., Ferland G. J., eds, Astrophysics of Gaseous Nebulae and Active Galactic Nuclei, 2nd edn. University Science Books, Mill Valley, CA  
 Panuzzo P., Bressan A., Granato G. L., Silva L., Danese L., 2003, A&A, 409, 99  
 Panuzzo P., Granato G. L., Buat V., Inoue A. K., Silva L., Iglesias-Páramo J., Bressan A., 2007, MNRAS, 375, 640  
 Pettini M., Pagel B. E. J., 2004, MNRAS, 348, L59 (PP04)  
 Pilyugin L. S., 2003, A&A, 399, 1003  
 Pilyugin L. S., Thuan T. X., 2005, ApJ, 631, 231  
 Quillen A. C., Yukita M., 2001, AJ, 121, 2095  
 Rieke G. H., Alonso-Herrero A., Weiner B. J., Pérez-González P. G., Blaylock M., Donley J. L., Marcillac D., 2009, ApJ, 692, 556  
 Salim S. et al., 2007, ApJS, 173, 267  
 Schlegel D. J., Finkbeiner D. P., Davis M., 1998, ApJ, 500, 525  
 Shao Z., Xiao Q., Shen S., Mo H. J., Xia X., Deng Z., 2007, ApJ, 659, 1159  
 Shi F., Kong X., Cheng F. Z., 2006, A&A, 453, 487  
 Shimabukuro K. et al., 2001, AJ, 122, 1238  
 Skillman E. D., Kennicutt R. C., Hodge P. W., 1989, ApJ, 347, 875  
 Sobral D., Best P., Matsuda Y., Smail I., Geach J., Cirasuolo M., 2011, MNRAS, in press (arXiv:1109.1830)  
 Somerville R. S., Primack J. R., 1999, MNRAS, 310, 1087  
 Stasińska G., Sodré L., Jr, 2001, A&A, 374, 919  
 Stasińska G., Mateus A., Jr, Sodré L., Jr, Szczepański R., 2004, A&A, 420, 475  
 Stasińska G., Cid Fernandes R., Mateus A., Sodré L., Asari N. V., 2006, MNRAS, 371, 972  
 Storchi-Bergmann T., Calzetti D., Kinney A. L., 1994, ApJ, 429, 572  
 Stoughton C. et al., 2002, AJ, 123, 485  
 Strateva I. et al., 2001, AJ, 122, 1861  
 Strauss M. A. et al., 2002, AJ, 124, 1810  
 Thomas H. C., Alexander P., Clemens M. S., Green D. A., Dunne L., Eales S., 2004, MNRAS, 351, 362  
 Tremonti C. A. et al., 2004, ApJ, 613, 898  
 Unterborn C. T., Ryden B. S., 2008, ApJ, 687, 976  
 Wang B., Heckman T. M., 1996, ApJ, 457, 645  
 Worthey G., Ottaviani D. L., 1997, ApJS, 111, 377  
 Wu H., Cao C., Hao C.-N., Liu F.-S., Wang J.-L., Xia X.-Y., Deng Z.-G., Young C. K.-S., 2005, ApJ, 632, L79  
 Yasuda N. et al., 2001, AJ, 122, 1104  
 Yip C.-W., Szalay A. S., Wyse R. F. G., Dobos L., Budavári T., Csabai I., 2010, ApJ, 709, 780  
 York D. G. et al., 2000, AJ, 120, 1579  
 Zahid H. J., Kewley L. J., Bresolin F., 2011, ApJ, 730, 137  
 Zaritsky D., Kennicutt R. C., Jr, Huchra J. P., 1994, ApJ, 420, 87  
 Zhou H., Wang T., Yuan W., Lu H., Dong X., Wang J., Lu Y., 2006, ApJS, 166, 128  
 Zhu Y.-N., Wu H., Cao C., Li H.-N., 2008, ApJ, 686, 155  
 Zoran O., Barkana R., Thompson R. I., 2006, MNRAS, 368, L47

This paper has been typeset from a TeX/LaTeX file prepared by the author.